STRUCTURAL BIOLOGY

Structural basis for the ubiquitination of G protein βγ subunits by KCTD5/Cullin3 E3 ligase

Wentong Jiang[1,2]†, Wei Wang[2,3]†, Yinfei Kong[4], Sanduo Zheng[1,2,5]*

G protein–coupled receptor (GPCR) signaling is precisely controlled to avoid overstimulation that results in detrimental consequences. Gβγ signaling is negatively regulated by a Cullin3 (Cul3)–dependent E3 ligase, KCTD5, which triggers ubiquitination and degradation of free Gβγ. Here, we report the cryo–electron microscopy structures of the KCTD5-Gβγ fusion complex and the KCTD7-Cul3 complex. KCTD5 in pentameric form engages symmetrically with five copies of Gβγ through its C-terminal domain. The unique pentameric assembly of the KCTD5/Cul3 E3 ligase places the ubiquitin-conjugating enzyme (E2) and the modification sites of Gβγ in close proximity and allows simultaneous transfer of ubiquitin from E2 to five Gβγ subunits. Moreover, we show that ubiquitination of Gβγ by KCTD5 is important for fine-tuning cyclic adenosine 3′,5′-monophosphate signaling of GPCRs. Our studies provide unprecedented insights into mechanisms of substrate recognition by unusual pentameric E3 ligases and highlight the KCTD family as emerging regulators of GPCR signaling.

INTRODUCTION

G protein–coupled receptors (GPCRs) transduce extracellular signals into intracellular responses through heterotrimeric G proteins comprising Gα, β, and γ subunits (*1*). The conformational change of GPCR upon agonist binding leads to the engagement of G proteins and the exchange of guanosine diphosphate for guanosine 5′-triphosphate (GTP) in Gα. GTP binding to Gα activates the G proteins by promoting the dissociation of Gα from the obligate Gβγ heterodimer, which exposes interaction interfaces of downstream effectors on Gβγ. The beta-bladed propeller structure of Gβ allows Gβγ to recruit a broad range of downstream effectors (*2*, *3*) including G protein–coupled inwardly rectifying potassium channel (GIRK) (*4*), voltage-gated calcium channel (*5*), adenylyl cyclase (AC) (*6*), and phospholipase C (*7*).

While GPCR signaling is essential for normal physiology, overstimulation or uncontrolled activation of GPCR leads to cellular toxicity and pathological conditions. The regulatory mechanisms that limit GPCR signaling and prevent overstimulation are referred to as desensitization (*8*, *9*). One well-established mechanism of GPCR desensitization is the activation-dependent regulation of receptors that involves GPCR kinases (GRK) and arrestins (*1*, *8*–*10*). Upon activation, receptors can recruit and activate GRKs, resulting in the phosphorylation of active GPCRs. GPCR phosphorylation subsequently engages arrestins, which prevent G protein coupling and reduce the number of receptors present on the cell surface by internalization. In addition to mechanisms that act on receptors, G protein signaling can be directly regulated. It has been shown that GRK can sequester both Gα and Gβγ and block their interactions with downstream effectors (*11*–*14*). A family of RGS (regulator of G protein signaling) proteins that includes at least 20 members and shares a characteristic RGS-homology domain promotes the inactivation of GTP-bound Gα by accelerating the guanosine triphosphatase activity of Gα (*15*, *16*). Despite the critical roles of Gβγ in GPCR signaling, little is known regarding the mechanisms by which Gβγ signaling is terminated. Until recently, members of the KCTD family have emerged as important regulators of Gβγ signaling.

The KCTD family contains more than 20 members, all of which share an N-terminal BTB (broad complex, tramtrack, and bric-a-brac) domain and have a variable C-terminal domain (CTD). The KCTD family has gained increasing attention because of their roles in fundamental biological processes and neurological disorders (*17*, *18*). For instance, more than 40 unique mutations in *KCTD7* have been identified in more than 50 patients with progressive myoclonic epilepsy (PME) (*17*). Copy-number variations in KCTD13 are associated with neurodevelopmental disorders such as autism and schizophrenia (*19*–*21*). The BTB domains in most, but not all, members of the KCTD family bind Cullin3 (Cul3) as 5:5 heterodecamers (*22*–*24*) and assemble into Cul3-RING E3 ligase (CRL3) with the RING domain protein Rbx1, while CTDs of KCTDs serve as substrate receptors. BTB domains in clade F of the KCTD family including KCTD8, KCTD12, and KCTD16 fail to associate with Cul3 (*22*, *23*), but instead bind to the C-terminal tail of γ-aminobutyric acid type B2 ($GABA_{B2}$) receptors as a homopentamer (*25*, *26*), and the CTD of KCTD12 can sequester Gβγ from GIRK to induce rapid desensitization of GIRK following $GABA_B$ activation (*25*, *27*, *28*). In contrast, KCTD2, KCTD5, and KCTD17 in clade E function as pentameric E3 ligases with Cul3. It has been recently shown that KCTD5 can terminate Gβγ signaling by triggering ubiquitination and degradation of free Gβγ dissociated from Gα (*29*, *30*). In striatal neurons, KCTD5 controls cyclic adenosine 3′,5′-monophosphate (cAMP) signaling of G_s-coupled receptors by Gβγ-mediated AC regulation (*31*). The physiological functions of KCTD5 have been well-studied in *Drosophila melanogaster*. The ortholog of KCTD5 in flies, Insomniac (Inc), together with Cul3 is essential for normal sleep regulation and retrograde homeostatic signaling (*32*–*36*). Epigenome-wide association analysis revealed the association between DNA methylation in *KCTD5* and daytime sleepiness (*37*). Moreover, KCTD2 and KCTD17 are genetically associated

[1]Graduate School of Peking Union Medical College, Beijing 100730, China. [2]National Institute of Biological Sciences, Beijing 102206, China. [3]School of Life Sciences, Peking University, Beijing 100871, China. [4]Peking-Tsinghua Center for Life Sciences, Academy for Advanced Interdisciplinary Studies, Peking University, Beijing 100871, China. [5]Tsinghua Institute of Multidisciplinary Biomedical Research, Tsinghua University, Beijing 100084, China.
*Corresponding author. Email: zhengsanduo@nibs.ac.cn
†These authors contributed equally to this work.

with Alzheimer's disease and myoclonus dystonia, respectively (*38*, *39*).

Our recently published structure of KCTD12 in complex with Gβγ has shown molecular details of interactions between KCTD12 and Gβγ (*25*). However, KCTD5 and KCTD12 share little sequence similarity in the CTD, although both bind to Gβγ. Moreover, it remains unclear how Cul3 is differentially recognized by the KCTD family members. Therefore, we sought to determine the structure of KCTDs in complex with its substrate and Cul3 to understand the molecular basis of the substrate ubiquitination by the pentameric KCTD/Cul3 E3 ligase.

RESULTS

Conserved binding interface between KCTDs and Gβγ during evolution

To determine which region of KCTD5 is involved in binding, we performed an in vitro pull-down assay using the FLAG-tagged KCTD5. The $G\beta_1\gamma_2$ heterodimer could be pulled down by the CTD of KCTD5 but not the BTB domain, suggesting that the CTD is essential and sufficient for binding Gβγ (Fig. 1A). Reminiscent of other subfamilies of closely related KCTD proteins such as KCTD8, KCTD12, and KCTD16, KCTD5, KCTD2, and KCTD17 share the high sequence similarity and interact with each other to form heteropentamers (fig. S1, A and B) (*40*). Consistent with previous studies (*30*), the pull-down assays showed that KCTD2 also forms detectable complexes with Gβγ (Fig. 1B). The human *KCTD17* gene has four protein isoforms with variable C termini following the CTD (fig. S1A). While the longer isoforms of KCTD17 (1 and 2) failed to form complexes with Gβγ, the shorter isoforms (3 and 4) could pull down Gβγ (Fig. 1B). This is analogous to KCTD8 and KCTD16 harboring an additional domain following the CTD of KCTD12, which prevents their interaction with Gβγ (*41*). $G\beta_2$, $G\beta_3$, and $G\beta_4$ that share high sequence identity with $G\beta_1$ but not $G\beta_5$ can be coimmunoprecipitated by KCTD5 (Fig. 1C and fig. S1C). Moreover, the *Drosophila* ortholog of KCTD5, Inc, can interact with the human $G\beta_1\gamma_2$, and the human KCTD5 can bind $G\beta_{13F}\gamma_{30a}$ in *Drosophila* that is closely related to Gβγ in humans but not a distal homolog $G\beta_{76C}$ (Fig. 1, B and D, and fig. S1D). These data suggest that Gβγ binding abilities of KCTDs and KCTDs-Gβγ interface are conserved during evolution.

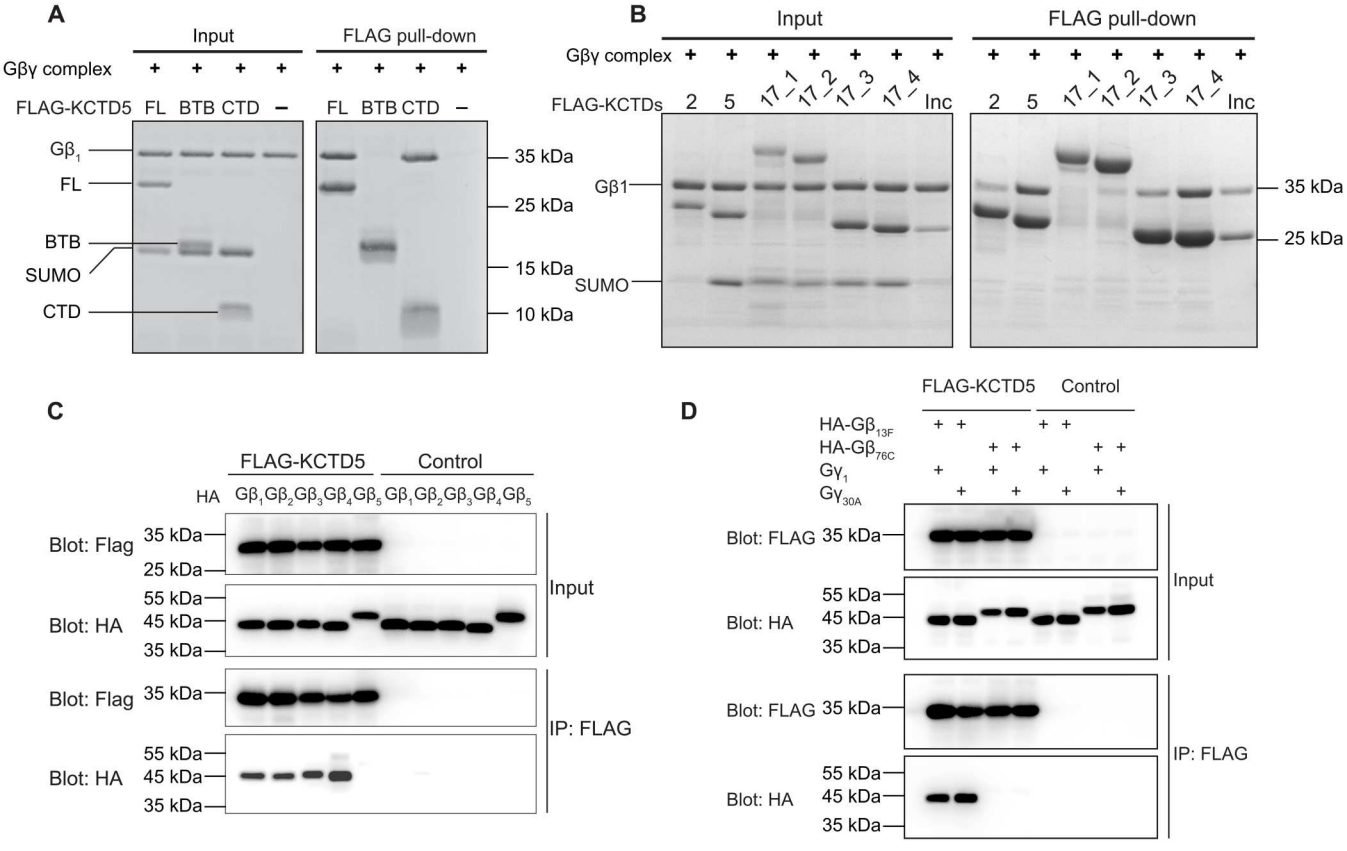

Fig. 1. Interaction analysis between KCTD2/5/17/Inc and Gβγ. (**A**) FLAG pull-down (PD) experiments. Purified His_6-SUMO-FLAG–tagged KCTD5 full-length (FL), BTB, or CTD was treated with ULP1, incubated with $G\beta_1\gamma_2$, and pulled down with M1 FLAG sepharose beads. The input and elution samples (FLAG PD) were resolved by SDS–polyacrylamide gel electrophoresis (PAGE) and stained by Coomassie blue. (**B**) FLAG PD experiments using the purified FLAG-tagged KCTDs and $G\beta_1\gamma_2$. 17_1 to 4 represent four isoforms of KCTD17. (**C**) Human embryonic kidney 293T cells were transfected with the FLAG-tagged KCTD5 and the hemagglutinin (HA)–tagged Gβγ subunits from *Homo sapiens*, lysed, and immunoprecipitated (IP) using anti-FLAG sepharose beads. The input samples and precipitates (IP) were subject to Western blot analysis. (**D**) Co-IP experiments with the FLAG-tagged KCTD5 and the HA-tagged Gβγ variants from *D. melanogaster*. Cells expressing Gβγ but not KCTD5 were used as a negative control. $G\beta_{13F}$ and $G\beta_{76C}$ are two Gβ homologs in *D. melanogaster*, and $G\gamma_1$ and $G\gamma_{30A}$ are two homologs of Gγ in *D. melanogaster*.

Structure determination of the KCTD5–Gβ$_1$γ$_2$ fusion complex

Structural characterization of E3 ligases in complex with their substrates has been challenging due to their weak and transient binding. Although KCTD5 and Gβγ can form a stable complex from the size exclusion chromatography (Fig. 2A), strong forces at the air-water interface led to the dissociation of the complex during cryo–electron microscopy (cryo-EM) grid preparation, resulting in heterogeneous particles and impeding structure determination. To enhance complex stability, we take advantage of the fusion protein strategy (*42*), where the N terminus of Gγ$_1$ is fused to the C terminus of KCTD5 (Fig. 2A). To avoid inappropriate linker length that may perturb the complex formation, we introduced a long linker including two 3C precision protease recognition sites with 25 residues. The linker between the two components brings them in close proximity and potentially increases their relative concentration and complex formation. Two-dimensional (2D) classification of the particles from this sample revealed symmetric starfish-like structures, indicating that KCTD5 forms 5:5 protein complexes with Gβγ (Fig. 2B). However, the pentameric KCTD5 is partially occupied by two or three copies of Gβγ in some 2D classes likely due to dissociation of some Gβγ or degradation of the linker. In line with 2D classification, ab initio 3D reconstructions generated multiple classes with KCTD5 fully or partially occupied by Gβγ (fig. S2A). Therefore, we implemented 3D classification without alignment to select particles with fully occupied Gβγ and were able to obtain a cryo-EM map of the KCTD5-Gβγ fusion complex at a global resolution of 3.3 Å by imposing C5 symmetry (Fig. 2, C and D, fig. S2B, and table S1). While side chains of most residues in Gβγ and the CTD of KCTD5 can be unambiguously modeled (fig. S2C), the BTB of KCTD5 is poorly defined owing to the high flexibility of the linker between the BTB and the CTD (Fig. 2C). This is consistent with previously determined crystal structures of KCTD5 that reveal two different orientations of the BTB domain and the CTD under different crystallization conditions (*43*) and molecular dynamics (MD) simulations showing the interdomain twisting motion in KCTD5 (*44*). As a result, the BTB domain was modeled on the basis of the crystal structure of KCTD5 (Fig. 2D).

Overall structure of KCTD5-Gβγ fusion complex

In agreement with biochemical data (Fig. 1A), the CTD of KCTD5 contributes most of the interactions with Gβγ. The CTD-Gβγ fusion complex assembles into a starfish-like structure with the pentameric CTD and five Gβγ subunits corresponding to the central disc and five arms, respectively (Fig. 2D). Gγ subunits are peripherally positioned on the edge of arms. The arrangement of the complex is compatible with the membrane anchoring of the Gγ subunit. The CTD in the complex resembles that in the crystal structure of KCTD5 alone (fig. S3A), and each subunit consists of a three-stranded antiparallel β sheet packing against α1 between β1 and β2 (Fig. 3A). KCTD5 binding also shows little influence on the conformation of Gβγ that forms a seven-bladed β-propeller (blades 1 to 7) fold. Contacts between Gβγ and CTD are constricted on Gβ, with each Gβ subunit interacting with two adjacent subunits of CTD (Fig. 3A). Despite their little sequence similarity, the CTD of KCTD5 shares a high structural similarity with the H1 domain of KCTD12 in the central region (fig. S3B). KCTD5 and KCTD12 likely share a common evolutionary origin and evolve distinct Gβγ binding modes for different functional purposes. The H1 of KCTD12 binds above blades 4, 5, and 6 of Gβ via its peripheral elements (α1, β2, and β3) (fig. S3, C to F) (*25*). However, the CTD of KCTD5 loses the peripheral elements and instead interacts with the side of the β-propeller of Gβ at blade 1 via α1 and β1 of the central region (Fig. 3A and fig. S3, D and E). Blade 1 is also involved in direct interactions with the N-terminal helix (αN) of the Gα subunit. Nevertheless, Gα occludes a larger surface on Gβγ than KCTD5 (1277 Å^2 versus 692 Å^2) (Fig. 3, B and C), which explains that KCTD5 can only target free Gβγ released from Gα. Moreover, KCTD12 engages a larger surface on Gβγ compared with both KCTD5 and GIRK (802 Å^2 versus 692 Å^2 and 434 Å^2) (Fig. 3B and fig. S3, F and H). Unlike the KCTD12-Gβγ complex where the Gβγ subunits interact extensively with one another (*25*), KCTD5 and GIRK (*45*) are bound by spatially isolated Gβγ subunits (Fig. 2D and fig. S3G). Few contacts are observed between neighboring Gβγ in the KCTD5-Gβγ fusion complex, and even mutations (R129A/E130A) in the contact did not influence KCTD5/Gβγ interaction (fig. S3, I and J). The relatively larger binding interface between KCTD12 and Gβγ and tightly packed Gβγ subunits when bound to KCTD12 allows a rapid and cooperative sequestration of Gβγ from GIRK by KCTD12. Given their similar architecture and their ability to bind Gβγ, the CTD of KCTD5, KCTD2, and KCTD17 and the H1 domain of KCTD12, KCTD8, and KCTD16 can be named G protein binding domain (GBD).

Detailed interactions between KCTD5 and Gβγ

Similar to the interactions between the GBD of KCTD12 and Gβγ (*25*), the GBD of KCTD5 mainly forms electrostatic interactions with Gβγ (Fig. 3D). R159 at one subunit of GBD forms a hydrogen bond with the backbone carbonyl group of L95 and salt bridge interactions with D76 at the blade 1 of Gβ, which also makes a hydrogen bond with S173 at the adjacent subunit of GBD. In addition, the aliphatic part of R159 and W179 engages hydrophobic interactions with P94 at Gβ (Fig. 3D). The GBD-Gβ interactions are further strengthened by hydrogen bond interactions between K78 and K89 at Gβ and the backbone carbonyl group of the GBD. In line with structural observations, mutations of these residues in either the GBD (R159, W179, and E167) of KCTD5 or Gβ (D76, K78, K89, and P94G) almost completely abolished their interactions in vitro (Fig. 3E and fig. S3J). Nevertheless, mutations of these residues in KCTD5 did not affect the interaction between KCTD5 and Cul3 (fig. S3K), indicating that these mutants are properly folded. Moreover, these essential residues of KCTD5 involved in binding Gβγ are conserved among KCTD2, KCTD5, KCTD17, and Inc, and residues of Gβ involved in binding KCTD5 are invariant among Gβ$_{1–4}$ in humans and Gβ$_{13F}$ in *Drosophila* (fig. S1, B and C). To further confirm whether their interactions are essential for KCTD-mediated Gβγ degradation, we performed the in vivo degradation assay in the engineered-HAPloid (eHAP) cell lines that predominantly express KCTD5 but not KCTD2 and KCTD17. As expected, knockout (KO) of the *KCTD5* gene in eHAP resulted in the elevated expression level of Gβ (fig. S3L), and overexpression of KCTD5 wild-type (WT) or KCTD5 mutants (E166A, S173A, and D177A) that can bind Gβγ in *KCTD5*-KO cell lines restored the expression level of Gβγ to WT (Fig. 3, E to G, and fig. S3M). In contrast, overexpression of KCTD5 mutants (R159A, E167A, and W179A) that cannot bind Gβγ failed to rescue the expression level of Gβγ (Fig. 3, E to G). The transfected KCTD5 WT and all mutants except E166A and E167A are expressed at comparable levels to the

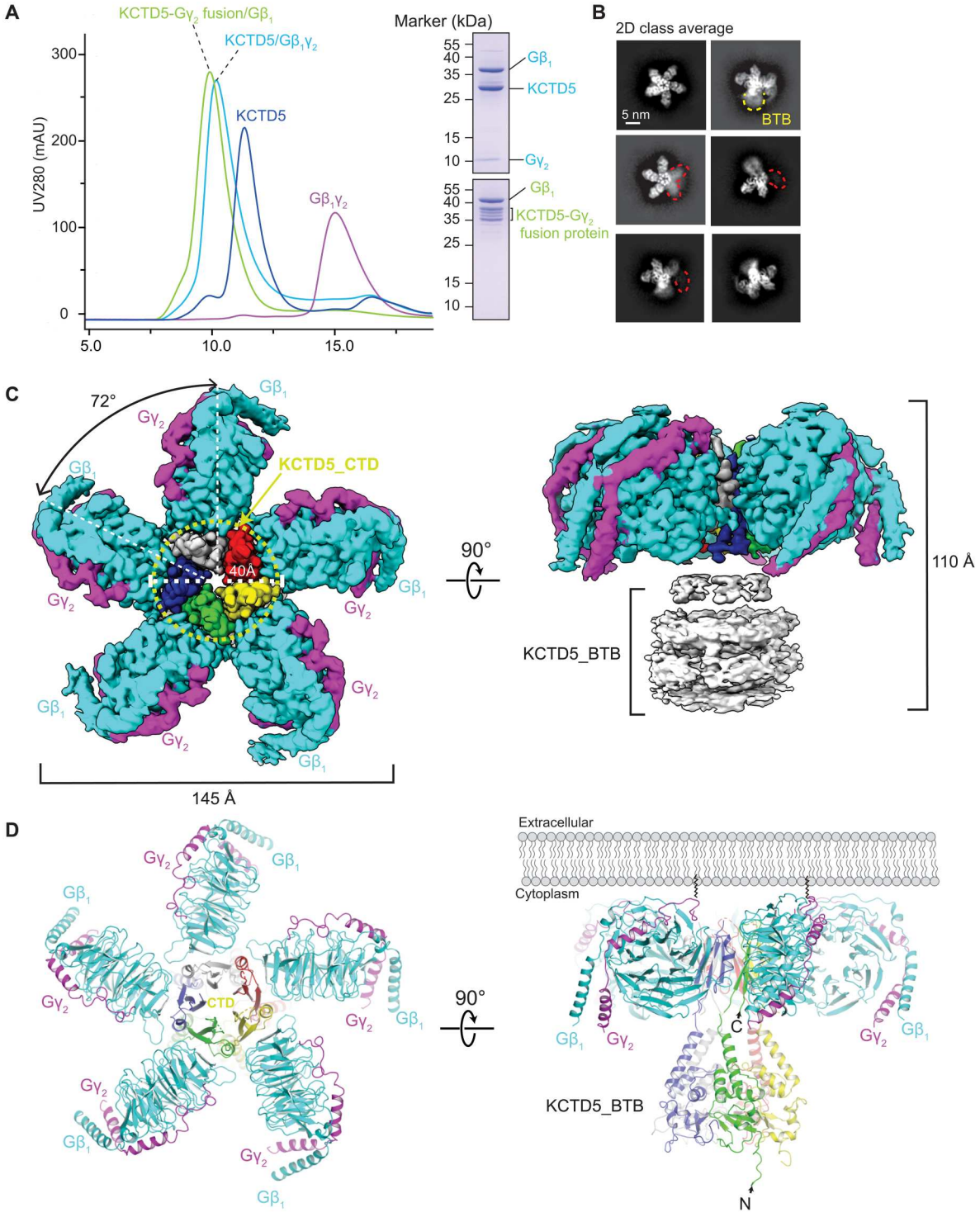

Fig. 2. Cryo-EM structure of KCTD5 in complex with $G\beta_1\gamma_2$. (**A**) Gel filtration analysis of individual components, the KCTD5-$G\beta_1\gamma_2$ complex, and the KCTD5-$G\gamma_2$ fusion protein and $G\beta_1$ complex. The complexes were resolved by SDS-PAGE and stained by Coomassie blue. (**B**) Representative 2D class average of the KCTD5-$G\gamma_2$ fusion protein and $G\beta_1$ complex. The blurring BTB domain and missing $G\beta\gamma$ subunits are outlined by yellow and red dashed lines, respectively. (**C**) Cryo–electron microscopy (cryo-EM) map of the KCTD5-$G\gamma_2$ fusion protein and $G\beta_1$ complex in two orthogonal views, with $G\beta_1$ shown in cyan, $G\gamma_2$ in magenta, and the CTD of KCTD5 in five different colors for each subunit. The EM map for the BTB domain of KCTD5 is shown in gray. (**D**) Overall structure of the KCTD5 and $G\beta_1\gamma_2$ complex in two orthogonal views. The CTD of KCTD5 and $G\beta_1\gamma_2$ is unambiguously modeled in the EM map. The BTB domain is modeled on the basis of the crystal structure of KCTD5 (Protein Data Bank: 3DRY). The black line represents the previously identified lipid modification of Gγ important for membrane anchoring.

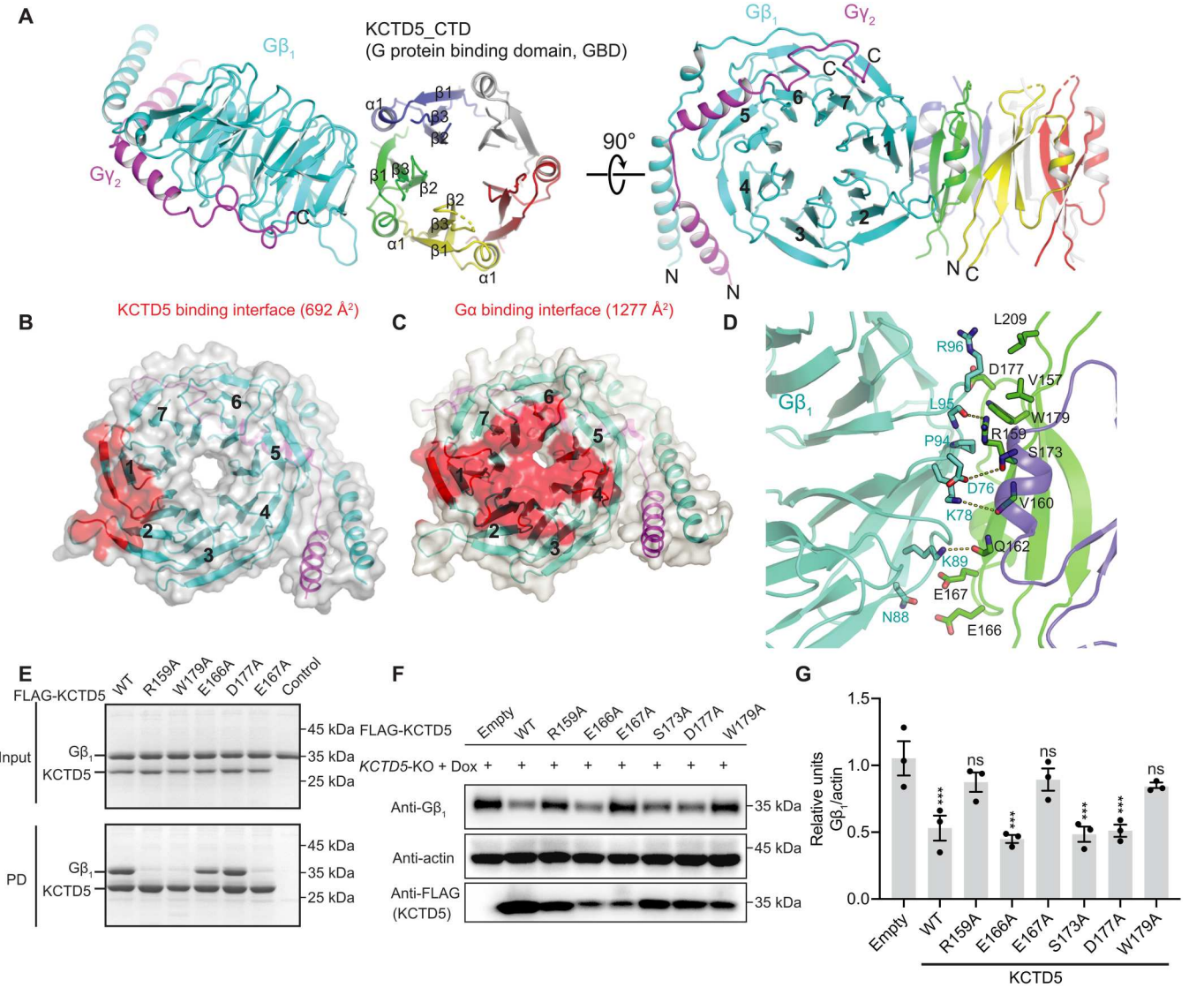

Fig. 3. Mechanism of Gβγ recognition by the CTD of KCTD5. (**A**) Structure of the CTD of KCTD5 and a copy of $G\beta_1\gamma_2$ in two orthogonal views. The seven blades of $G\beta_1\gamma_2$ are labeled. (**B** and **C**) Surface views of $G\beta_1\gamma_2$ with KCTD5 (B) and Gα (C) binding interface colored in red. (**D**) Detailed interaction between $G\beta_1$ and two subunits of the G protein binding domain (GBD) of KCTD5. The dashed line represents the hydrogen bond. (**E**) FLAG PD experiments between Gβγ and the wild-type (WT) or mutants of FLAG-tagged KCTD5. The input and PD samples were resolved by SDS-PAGE and stained with Coomassie blue. (**F** and **G**) Effect of mutations in the interface of KCTD5 and Gβγ on Gβγ degradation. The *KCTD5*-KO engineered-HAPloid (eHAP) cell lines were stably transfected with the FLAG-tagged KCTD5 WT or mutants under a doxycycline (Dox)–inducible expression system. Empty indicates the empty plasmid without KCTD5. The expression levels of $G\beta_1$ and KCTD5 were analyzed by Western blot using anti-β_1 and anti-FLAG antibodies, respectively (F). Actin was used as a loading control. Bands corresponding to $G\beta_1$ were quantified using ImageJ and normalized to the corresponding actin band (G). Statistical analysis was performed from three independent experiments with the one-way analysis of variance (ANOVA) method (***$P < 0.001$; ns, not significant).

endogenous KCTD5 (fig. S3N). Together, these data indicate that the interaction between KCTD5 and Gβγ is required for robust degradation of Gβγ by KCTD5.

Cul3 recognition by pentameric BTB domains in the KCTD family

Some CRL3 members such as Speckle Type BTB/POZ Protein (SPOP) and Kelch-like ECH-associated protein 1 (KEAP1) form an obligate dimer via the BTB domain and bind two degrons in a single-substrate polypeptide through their substrate-binding domains (*46*). The dimeric BTB domains separately recruit two Cul3 subunits together with a "3-box" motif following the BTB domain (*47*, *48*), which is absent in the pentameric BTB domains. Although homology modeling using the dimeric BTB domain bound to Cul3 and mutagenesis studies have revealed essential residues involved in binding (*22*–*24*), molecular details of Cul3 binding with the BTB domain of KCTDs remain poorly defined at the atomic level. Our attempt to determine the cryo-EM structure of KCTD5-Gβγ-Cul3 failed because of their instability and orientation preference. Instead, we were able to obtain the cryo-EM

structure of KCTD7 in complex with the N-terminal domain (NTD) of Cul3 with an overall resolution of 2.9 Å (fig. S4 and table S1). The high-resolution EM map enables us to precisely model most regions of KCTD7 and the N-terminal region of Cul3 involved in binding KCTD7 (Fig. 4A and fig. S4E). Similar to the organization of the GBD domain of KCTD5 and Gβγ complex, the pentameric BTB domain of KCTD7 sits at the fivefold axis with five arms corresponding to Cul3, extended from the BTB domain (Fig. 4B). Each Cul3 simultaneously interacts with distinct interfaces of the two adjacent BTB subunits of KCTD7, named the primary and the secondary binding interfaces, which bury total surface areas of 732 and 247 $Å^2$, respectively (Fig. 5A). The primary binding interface between one BTB subunit and Cul3 is equivalent to that observed between Cul3 and the dimeric BTB domain, while the secondary binding interface between Cul3 and the adjacent BTB subunit may compensate for the loss of the 3-box motif (fig. S5, A and B). The primary binding interface mainly involves hydrophobic interactions between a stretch of aromatic residues including F54, Y58, and Y62 lining the H2 of Cul3, as well as M76 and Y131 in α2 and α4 of BTB (Fig. 5A). Mutation of M76 or Y131 in KCTD7 markedly impairs the interaction between KCTD7 and Cul3, as shown by the in vitro pull-down assay (Fig. 5B). Notably, Y131 is conserved among all KCTD members, whereas the equivalent residues of M76 are either M or F in Cul3 binders including KCTD2/5/17/3/10/13/6/11/21 but are changed to basic residues (K or R) or relatively smaller hydrophobic residues (T or L) in non-Cul3 binders such as KCTD14/1/15/8/12/16 (fig. S5, C and D) (*22*–*24*), which should weaken the hydrophobic interactions and contribute to their inability to bind Cul3. In addition, the salt bridge and hydrophobic interactions between R84 and H85 in the variable α2-β3 loop of BTB, and D121 and F54 of Cul3 are critical for KCTD7 and Cul3 interaction, as mutation of R84 or H85 in KCTD7 impairs their binding (Fig. 5, A and B). Both are conserved in some Cul3 binders such as KCTD3 (R/I), SHKBP1 (R/I), KCTD10 (R/M), and KCTD13 (R/V), but only the hydrophobic residues equivalent to H85 are present in KCTD2/5/17 (fig. S5D). Nevertheless, a stretch of acidic residues present in the longer α2-β3 loop of KCTD2/5/17 may create additional contact with Cul3 and substitute for the absence of the salt bridge interaction. The secondary binding interface plays a minor role in KCTD7 and Cul3 interaction since disruptions of this interface (R65A or S67A) showed little effect on their binding (Fig. 5B). Noteworthily, the crystal structure of the BTB domain of KCTD16 that engages the C-terminal tail of the $GABA_{B2}$ receptor and the BTB domain of KCTD1 reveals an open pentamer (fig. S6, A to C), which is not compatible for Cul3 binding and may also contribute their inability to bind Cul3.

Despite their little sequence similarity, the CTD of KCTD7 retains structural elements of the CTD in KCTD5, where three antiparallel β sheet packs against one helix (Fig. 5, C and D, and fig. S5G). In contrast to the flexible linker between BTB and CTD in KCTD5 or KCTD12, the equivalent linker in KCTD7 forms an

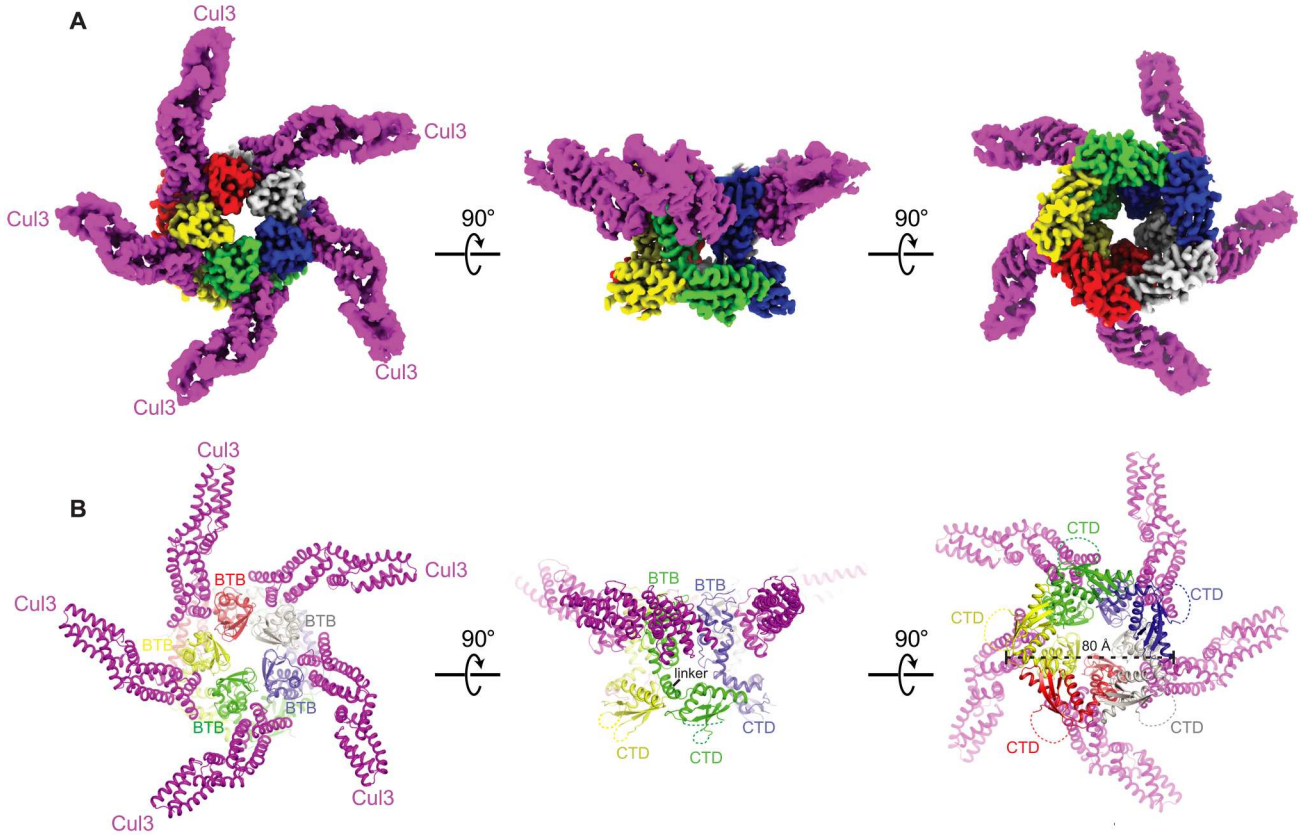

Fig. 4. Cryo-EM structure of the KCTD7 and Cul3 complex. (**A**) Cryo-EM map of the KCTD7 and Cul3 complex in three different views. Five copies of Cul3 are colored in magenta, and five subunits of KCTD7 are in five different colors. (**B**) Structure of the KCTD7 and Cul3 complex in three different views.

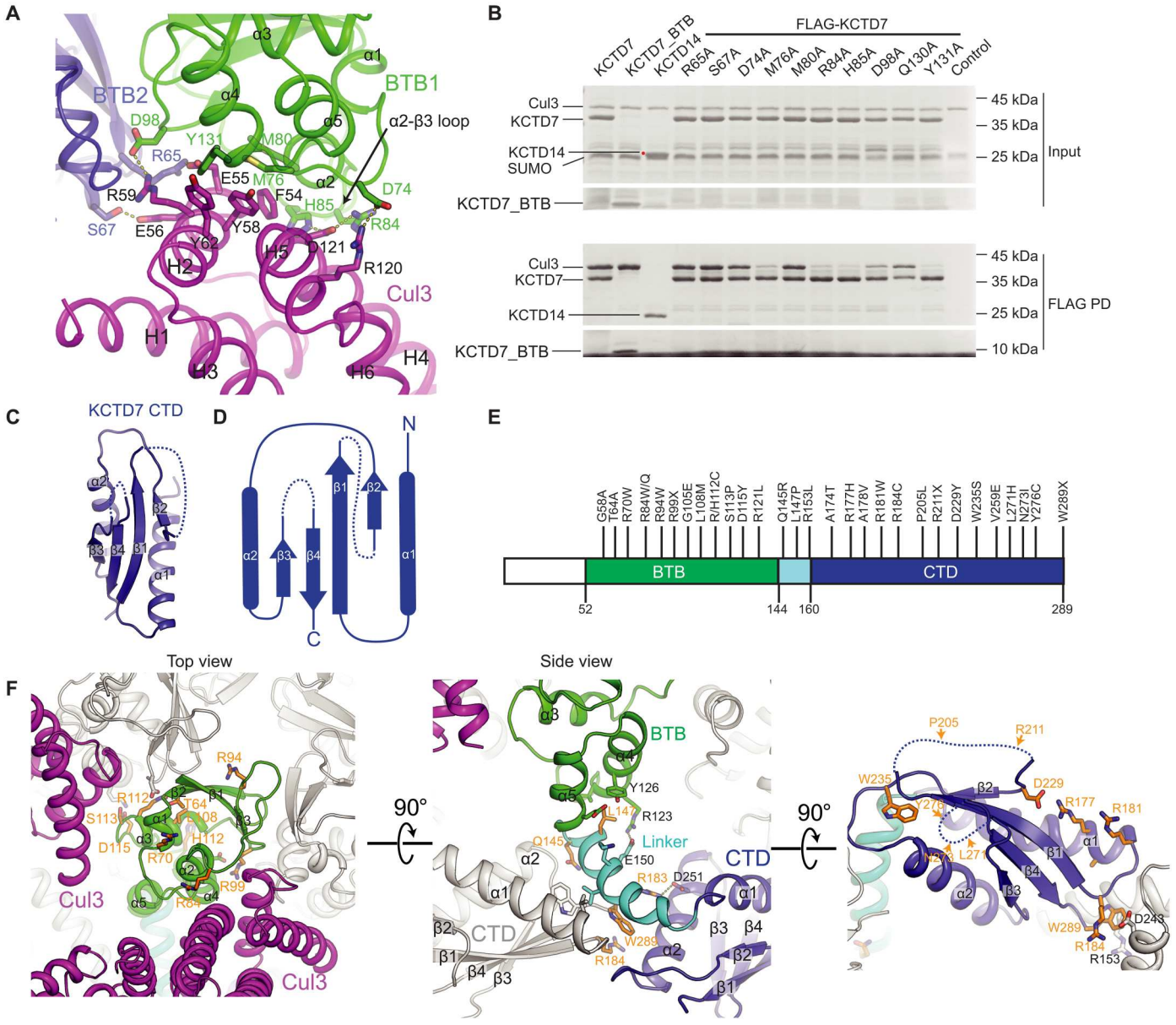

Fig. 5. Mechanisms of Cul3 recognition by the BTB domain of KCTD7 and PME disease associated with *KCTD7* mutations. (**A**) Detailed interactions between KCTD7 and Cul3. Each Cul3 contacts two adjacent BTB subunits of KCTD7. (**B**) FLAG PD experiments between Cul3 and the FLAG-tagged KCTD7 (WT or mutants) or KCTD14. Control indicates Cul3 only without Flag-tagged KCTD7. The contaminant is an unknown protein that is copurified with Cul3 from bacteria. The input and FLAG PD samples were resolved by SDS-PAGE and stained with Coomassie blue. (**C**) Structure of the CTD domain of KCTD7. (**D**) Topology diagram of the KCTD7 CTD structure. (**E**) Location of *KCTD7* PME mutations on the primary *KCTD7* sequence from *Mus Musculus*. (**F**) Mapping of PME mutations onto the structure of the KCTD7 and Cul3 complex in three different views. Mutant residues are shown in orange. The BTB domain, the linker, and the CTD of one KCTD7 subunit are colored in green, cyan, and blue, respectively, and the other four subunits are in gray. Mutations in the disorder region (represented by a dashed line) of the CTD domain of KCTD7 are labeled with arrows.

alpha-helical structure and is wedged between two neighboring CTDs, thereby promoting the CTD oligomerization and leading to a different oligomeric interface (Fig. 4B). The CTDs in other KCTD members such as KCTD1 in clade A and KCTD6 in clade B also have structural elements of KCTD5 CTD and acquire additional structural elements between β1 and α1 (fig. S6, D to H), which are possibly involved in binding different substrates. Despite the availability of the AlphaFold structures, the oligomerization interfaces of these KCTDs still require further structural characterization. These structural findings suggest that most KCTD family members may share a common ancestor. The structure of KCTD7-Cul3 also allows us to interrogate possible mechanisms of PME diseases caused by *KCTD7* mutations. On the basis of their functions, all these mutations can be divided into four groups (Fig. 5, E and F): (i) mutations in residues that are buried in the protein interior and are essential for protein folding such

as T64, L108, L147, and W235; (ii) mutations in residues involved in oligomerization formation (e.g., R94, R112, S113, D115, Q145, R183, R184, and W289); (iii) mutations in residues involved in Cul3 binding including aforementioned R84; (iv) mutations in residues that are located in the disorder region of CTD (e.g., P205, R211, L271, and N273) and possibly involved in substrate binding. It is noteworthy that W289, the last residue of KCTD7 is sandwiched by R184 in the CTD and R183 in the linker region of the adjacent subunit (Fig. 5F). Mutations of any of the three residues would destabilize the oligomer, thereby leading to PME. Together, the structure of KCTD7-Cul3 provides a plausible explanation for how Cul3 is differentially recognized by the KCTD family members and how *KCTD7* mutations cause PME diseases.

Mechanisms of Gβγ ubiquitination by KCTD5

Given the high sequence similarity between BTB domains of KCTDs, we generated a homology model of KCTD5-Cul3 using the cryo-EM structure of the KCTD7 and Cul3 complex (fig. S7A). The KCTD5-Cul3-NEDD8-RBX1-E2-Ub complex was modeled by using the cryo-EM structure of Cul1-NEDD8-RBX1-Ub-UBE2D2 [Protein Data Bank (PDB): 6TTU] (*49*) as a template (Fig. 6, A to C). Similar to the structure of KCTD7 and Cul3, the NTD of Cul3 interacts with the oligomerization interface of the BTB domain in KCTD5 through a mix of aromatic and polar interactions (Fig. 6, C and D, and fig. S7B). As expected, aromatic interactions between F128 and F69 in the BTB domain and F54, Y58, and Y61 in α2 of Cul3 play an essential role in their interaction, as mutation of F128 or F69 in KCTD5 impairs their interaction, while mutation of R72 or D93 shows little effect on their binding (fig. S7C). This is consistent with previous studies showing that the F128 mutation markedly reduced the binding affinity between KCTD5 and Cul3 (*23*). These KCTD5 mutants can interact with Gβγ, suggesting that they are properly folded (fig. S7C). Consistently, in contrast to the R72A and D93A mutants, the F69A or F128A mutant of KCTD5 failed to restore the expression level of Gβγ to WT (Fig. 6, F and G). The long stalk-like NTD of Cul3 positions five catalytic modules (E2-Ub) to surround five copies of Gβγ substrates, which juxtaposes each catalytic module and its corresponding substrate (Fig. 6, A and B). The pentameric assembly of CRL3 possibly enables simultaneous recruitment and ubiquitination of five substrates. Two previously identified acceptor lysines (*29*, *30*), K23 in $G\beta_1$ and K29 in $G\gamma_2$, are in closer proximity to the active site (C85) in E2 compared with other lysines in Gβγ (Fig. 6, A and B). The distance between them is around 30 Å (Fig. 6E), which still exceeds the distance required for Ub transfer. However, the dynamic nature of the winged-helix B (WHB) domain of Cul3, RBX1, and NEDD8 (*49*) as well as the flexible linker between BTB and GBD domain of KCTD5 (*44*) could further shorten the distance between the acceptor lysine and active site of E2. To understand the dynamics of KCTD-containing E3 ligases, we further performed MD simulations using the structural model of KCTD5/Cul3/Rbx1 and Gβγ (fig. S7, E to G). The distance between the ubiquitination site K23 of Gβ and the neighboring residue R714 of Cul3 can fluctuate between 6 and 60 Å (fig. S7, H to L). Therefore, the high conformational flexibility of the KCTD5-containing E3 ligase makes it possible to transfer Ub from the active site of E2 to K23 of Gβ and K29 of Gγ.

Regulation of cAMP signaling by KCTD-mediated Gβγ degradation

Most downstream effectors bind to the top of the Gβ torus termed the "hotspot" region where the switch II region of Gα contacts (fig. S7D). Although KCTD5 interacts with the side of the Gβ torus, the hotspots region of Gβ is occluded from effector binding by the adjacent Gβγ subunit. Therefore, KCTD5 is not compatible with other downstream effectors for binding Gβγ. Previous studies have shown that activated $G\alpha_s$ and free Gβγ act synergistically to activate particular types of AC (*6*). In primary striatum neurons, KCTD2, KCTD5, or KCTD17 decreases cAMP production stimulated by G_s-coupled receptors such as the D1 dopamine receptor (D1R) by degrading free Gβγ (*31*). To further validate our structural observations and investigate the functional relevance of KCTDs-mediated Gβγ degradation, we performed a cAMP accumulation assay in eHAP cells heterologously expressing D1R. Consistently, KO of *KCTD5* accelerates the production of cAMP and increases the maximal response of cAMP accumulation stimulated by dopamine (Fig. 7A and fig. S7M). Overexpression of KCTD5, KCTD2, or short isoforms of KCTD17 (3 and 4) that can bind both Gβγ and Cul3 in *KCTD5*-KO cells restored the cAMP level to WT (Fig. 7, A and B, and fig. S7M). In contrast, overexpression of KCTD5 mutants (F128A, R159A, E167A, and W179A) or long isoforms of KCTD17 (1 and 2) that fail to interact with either Gβγ or Cul3 cannot restore the cAMP level. Similarly, KCTD12 that can bind Gβγ but cannot trigger its degradation did not rescue the cAMP level of *KCTD5*-KO cells to WT. These results indicate that KCTD-mediated Gβγ degradation is critical for fine-tuning cAMP signaling.

DISCUSSION

Our work provides a framework for understanding how the substrate is recognized and ubiquitinated by this unusual family of KCTD-containing CRL3 E3 ligases that oligomerize into pentameric form and underscores the importance of the ubiquitin (Ub)–proteasome pathway in GPCR desensitization. We further described the biophysical characterization of *KCTD7* mutations causing PME diseases. These mutations can either destabilize its folding and oligomerization or impair its interaction with Cul3 or substrates. Although KCTD5 engages five identical substrates in our structure, it is possible that KCTDs can recruit less than five substrates or several distinct substrates for ubiquitination, as evidenced by the fact that KCTD5 with partially occupied Gβγ exists in our cryo-EM sample (fig. S2A). In contrast to most CRLs E3 ligases that are either monomeric or dimeric, and ubiquitinate a single substrate (*46*), the pentameric assembly of the KCTD family could enhance the efficiency of ubiquitination and degradation of substrates such as Gβγ that are abundantly present and need to be rapidly degraded to avoid excessive signaling. While most other CRLs specifically recognize flexible motifs known as "degrons" (*46*, *50*), KCTD5 binds to the folded region of the substrate (Fig. 3A), suggesting that the KCTD family may be adapted for substrates that have no recognizable disorder motif or degron. Moreover, the interface of KCTD5 and Gβγ could create a deep pocket for the development of molecular glues that enhance KCTD5 and Gβγ interaction and promote Gβγ degradation (fig. S7D), which provides a therapeutic strategy for diseases that are associated with Gβγ hypersignaling (*3*).

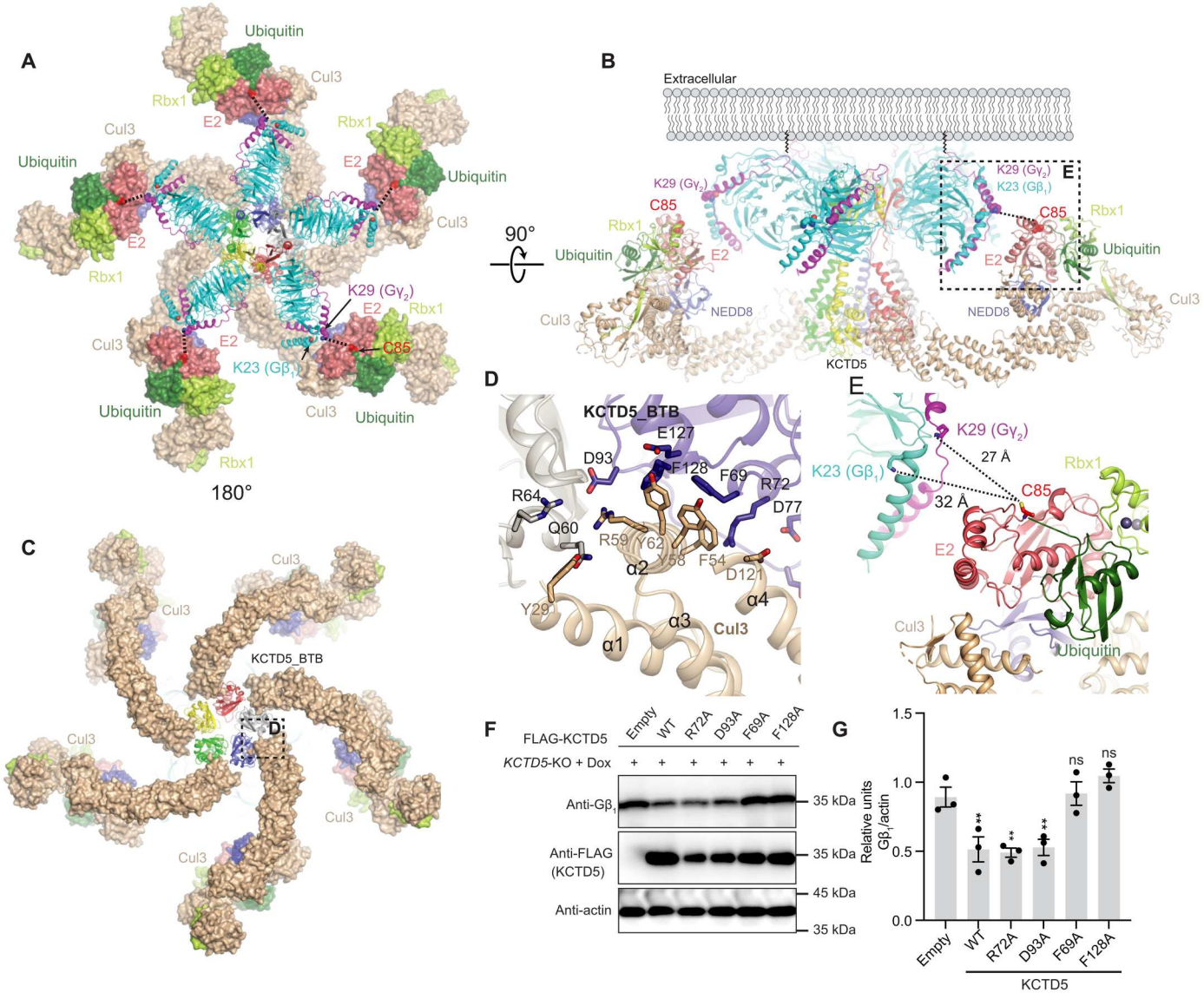

Fig. 6. Mechanism of Gβγ ubiquitination by the KCTD5/Cul3/Rbx1 E3 ligase. (**A** to **C**) Structure of E3 ligase (Cul3-NEDD8-Rbx1-KCTD5) and E2-Ub in complex with the substrate Gβγ in three different views. The ubiquitin-modified residues (K23 and K29) in Gβγ and the active site of E2 (C85) are shown as spheres and labeled. Three copies of Cul3/Rbx1/NEDD8/E2/Ub in (B) are omitted for clarity. (**D**) Detailed interactions between Cul3 and the BTB domain of KCTD5. (**E**) The ubiquitin-modified lysine (K23 and K29) are in close proximity to the active site of E2. (**F** and **G**) Effect of mutations in the interface of KCTD5 and Cul3 on Gβγ degradation. The *KCTD5*-KO eHAP cell lines were stably transfected with the FLAG-tagged KCTD5 WT or mutants under a Dox-inducible expression system. The expression levels of $G\beta_1$ and KCTD5 were analyzed by Western blot with actin as a loading control. Bands corresponding to $G\beta_1$ were quantified using ImageJ and normalized to the corresponding actin. Statistical analysis was performed from three independent experiments with the one-way ANOVA method (**$P < 0.01$).

GPCR desensitization mediated by the KCTD family members through distinct mechanisms

Although KCTD12 and KCTD2/5/17 can induce GPCR desensitization through binding Gβγ, they evolved distinct binding modes with Gβγ for different functional purposes. The ability of the BTB domain in KCTD2/5/17 to interact with Cul3 and the unique Gβγ binding mode of the CTD or GBD place the substrate lysines in close proximity to E2, leading to ubiquitination and degradation of Gβγ. The high-affinity binding of the BTB domain of KCTD12 with the C-terminal tail of the $GABA_{B2}$ subunit endows KCTD12 to specifically desensitize the $GABA_B$ receptor and is required for tethering KCTD12 to the membrane to sequester Gβγ from GIRK via its GBD domain (*27*). However, it is unclear whether KCTD2/5/17 regulates specific GPCRs and how KCTD5 is trafficked to the membrane before binding and ubiquitinating free Gβγ. Recent studies have shown that Inc and Cul3 are translocated to the postsynaptic compartments and promote local mono-ubiquitination following the perturbation of glutamate receptors (*33*). Therefore, it is likely that certain stimuli and membrane-anchored adaptors are required for the recruitment of KCTD5 to the membrane and its interaction with Gβγ given the weak binding affinity between KCTD5 and Gβγ.

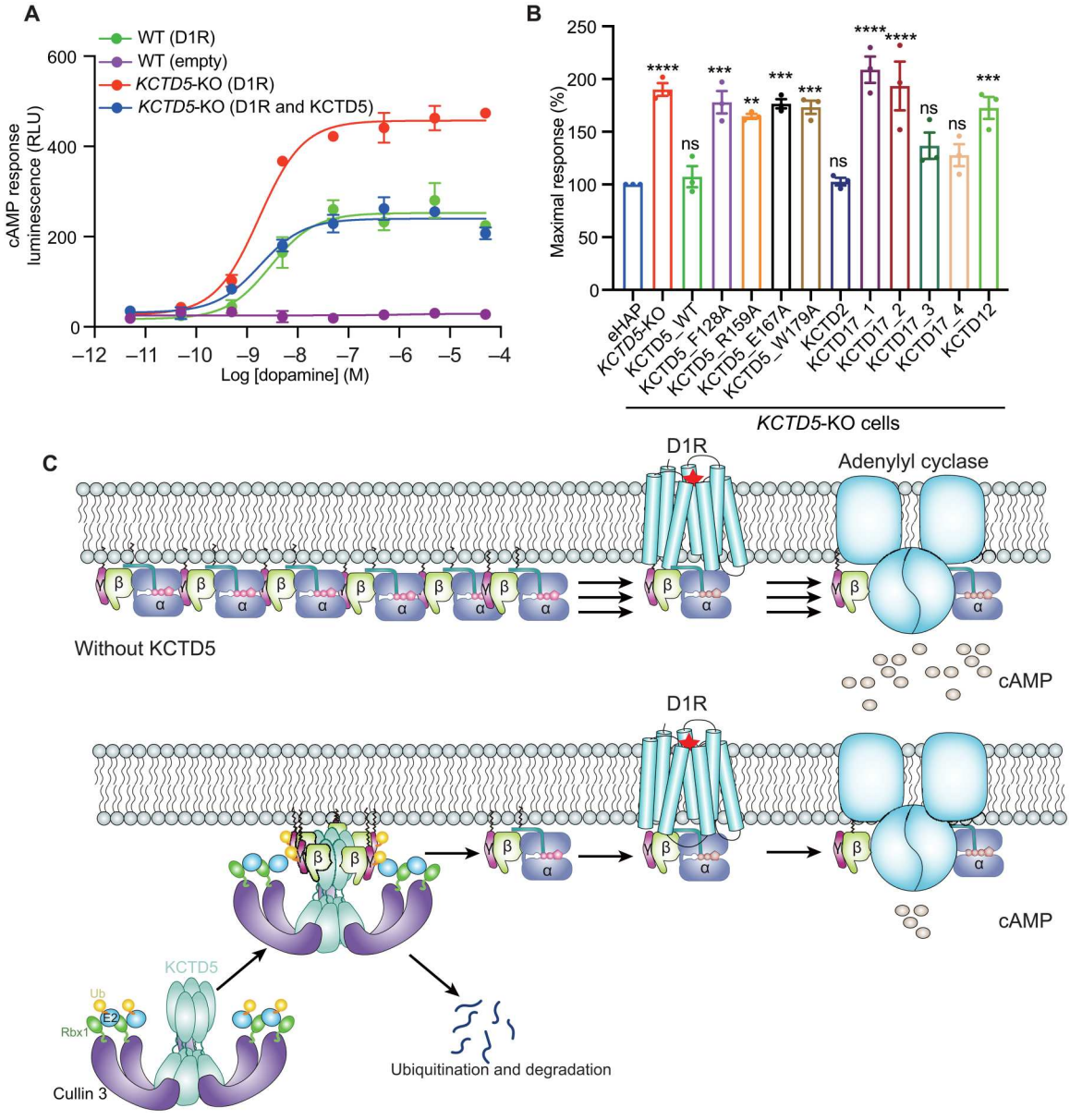

Fig. 7. KCTD2, KCTD5, and KCTD17 regulate cAMP signaling. (**A**) Concentration-response curves of dopamine-induced AMP accumulation in eHAP cells (WT) transfected with D1R or in *KCTD5*-KO cells transfected with D1R only or both D1R and KCTD5. (**B**) Summary of the maximal dopamine-induced responses in *KCTD5*-KO cells transfected with D1R and KCTDs WT or with D1R and KCTD5 mutants. All maximal responses are normalized as the percentage of the maximal dopamine-induced response in eHAP cells transfected with D1R. Statistical analysis was performed from three independent experiments with the one-way ANOVA method (*$P < 0.05$, **$P < 0.01$, ***$P < 0.001$, and ****$P < 0.0001$). (**C**) Proposed model for GPCR desensitization by KCTD5. In the case of D1R, its activation by agonists leads to the dissociation of Gβγ from $G\alpha_s$. Activated $G\alpha_s$ subunit together with the released Gβγ activates AC, resulting in the production of cAMP. The basal activities of D1R and endogenous GPCRs can liberate Gβγ, which are targeted by the cytosolic KCTD5/Cul3/Rbx1 E3 ligase for ubiquitination and degradation. As a result, KCTD5 decreases the basal levels of Gβγ and thus limits the amounts of Gαβγ available for D1R and AC, leading to a reduced amount of cAMP.

While Gβγ binding with KCTD12 is reversible (*27*) and can be completed through reassociation with Gα, KCTD5 irreversibly degrades the activated Gβγ subunits, limiting the amount of free Gβγ for activating downstream effectors such as AC and leading to long-term desensitization (Fig. 7C). Reminiscent of arrestins that prevent G protein binding with receptors in addition to reduce the receptor levels in the membrane, KCTD5 could possibly prevent Gβγ binding with downstream effectors, engendering short-term desensitization. In addition to Gβγ, RhoA that can be regulated by some GPCRs through the $G\alpha_{12/13}$ pathway is targeted by KCTD13/BACURD for degradation (*51*). The KCTD13-Cul3-RhoA pathway has been shown to be associated with neurodevelopment and psychiatric diseases (*19*–*21*). However, it remains to be elucidated whether other KCTD members can regulate GPCR signaling since the substrates of most other KCTD members have not been characterized. Identification of their substrates in the future

will be important in understanding molecular mechanisms underlying neuropsychiatric diseases and the development of modern therapeutics against them.

Implications in physiological functions of the KCTD5-Cul3-Gβγ pathway

Our studies suggested that Gβγ could be a possible target of KCTD5 responsible for normal sleep regulation. First, our structures revealed that the KCTD-Gβγ interaction interface is conserved during evolution from worms, flies, to humans (fig. S1, B and C). Knockdown or KO of the homologs of *KCTD5* and *Cul3* in worms (*52*) or flies (*34*, *36*) reduced sleep time. KCTD5 can interact with $G\beta_{13F}\gamma_{30a}$ in *Drosophila*, and the human KCTD2 and KCTD5 restore normal sleep of *Inc* mutants (*32*). Second, R159 in KCTD5 is involved in interaction with Gβγ; mutation of R159 in KCTD5 abolished their interaction, and the R135H mutant (equivalent residue of R159) of Inc was unable to restore sleep to *Inc* mutants (*35*). Third, it has been shown that Cul3/Inc functions in a dopaminergic arousal pathway (*36*); given that many GPCRs such as orexin receptors (*53*, *54*) and cAMP signaling (*55*) have been implicated in sleep regulation, it would be expected that KCTD-mediated Gβγ degradation plays a role in sleep. Clearly, future studies are required to clarify if KCTD2/5/17 regulates sleep in mammals and if Gβγ is the direct target of KCTD2/5/17/Inc for sleep regulation.

METHODS

Protein expression and purification

For expression and purification of the KCTD5 protein, the mouse *KCTD5* gene was amplified from a C57BL/6N brain cDNA library and cloned into a pET28a(+) plasmid with an N-terminal His_6-SUMO followed by a FLAG tag (DYKDDDDK). The plasmid was transformed into *Escherichia coli* strain BL21 (DE3). Bacteria were cultured at 37°C to reach an OD_{600} (optical density at 600 nm) of 0.6 to 0.8 and induced with 0.5 mM isopropyl 1-thio-β-glucopyranoside at 18°C for 18 hours. Pelleted cells were harvested by centrifugation and resuspended in lysis buffer A [50 mM tris (pH 8.0), 250 mM NaCl, and 25 mM imidazole) for sonication. The lysate was clarified by centrifugation at 38,000*g* for 30 min and loaded onto a nickel–nitrilotriacetic acid (Ni-NTA) column pre-equilibrated with lysis buffer A. The bound fraction was washed with 50 column volumes of lysis buffer A and eluted with elution buffer A (lysis buffer A supplemented with 300 mM imidazole). The eluate was then incubated overnight with Ubl-specific protease 1 (ULP1) to remove the His_6-SUMO tag at 4°C, flash-frozen in liquid nitrogen, and stored at −80°C for further experiments.

The human $G\beta_1$ and $G\gamma_2$ (C68S) were cloned into a pFastBac-Dual vector and expressed in Tni insect cells (Expression Systems) using the Bac-to-Bac baculovirus system. Cells were infected with baculovirus when cells reached a density of 3×10^6 per ml. After shaking at 27°C for 48 hours, cells were harvested by centrifugation and were lysed by a Dounce homogenizer in lysis buffer A. Cell lysate was clarified by centrifugation at 38,000*g* for 30 min, and the supernatant was filtered and loaded onto a Ni-NTA column by gravity. The resin was washed extensively with lysis buffer A and eluted with elution buffer A. The eluted proteins were purified by HiTrap Q HP anion exchange chromatography (Cytiva) followed by size exclusion chromatography on a Superdex 200 Increase 10/300 column (Cytiva) in equilibrate buffer A [25 mM Hepes (pH 7.4) and 150 mM NaCl]. To assemble the KCTD5/Gβγ complex, purified KCTD5 and Gβγ proteins were mixed with a molar ratio of 1:1.2 and incubated on ice for 5 min before further purification using a Superdex 200 Increase 10/300 column (Cytiva) equilibrated in equilibration buffer B [20 mM Hepes (pH 7.4) and 80 mM NaCl].

For expression and purification of the KCTD5-$G\gamma_2$ fusion protein and $G\beta_1$ complex, the fragments encoding *KCTD5* and $G\gamma_2$ (C68S) were cloned into pcDNA3.1(+) (Thermo Fisher Scientific) interspaced with two 3C precision sites (LEVLFQGP) with a His_6 tag and a protein C tag (EDQVDPRLIDGK) at the N terminus of KCTD5 for affinity purification. $G\beta_1$ gene was cloned into the pcS2 plasmid with an N-terminal 3x human influenza hemagglutinin tag (HA; YPYDVPDYA). The two plasmids were cotransfected into Expi293F cells (Thermo Fisher Scientific) using polyethyleneimine max (PEI; Polysciences) at a cell density of 1.5 million per milliliter and cultured for 2 days. Cells were pelleted and lysed in lysis buffer B [20 mM Hepes (pH 7.4), 150 mM NaCl, and 20 mM imidazole) through sonication. The lysate was clarified by centrifugation and subjected to a tandem affinity purification procedure. The lysate was bound to a Ni-NTA column equilibrated with lysis buffer B and eluted with elution buffer B (lysis buffer B supplemented with 250 mM imidazole). The eluate was then supplemented with 2 mM $CaCl_2$ and applied onto protein C antibody affinity resin. The bound fraction was washed with equilibration buffer A supplemented with 2 mM $CaCl_2$ and eluted with equilibration buffer A supplemented with 5 mM EDTA and protein C peptide (0.1 mg/ml). The eluate was concentrated and subjected to a Superdex 200 Increase 10/300 column (Cytiva) equilibrated in equilibration buffer A. The peak fraction corresponding to KCTD5-$G\gamma_2/G\beta_1$ was verified by SDS–polyacrylamide gel electrophoresis (PAGE) and concentrated to 0.69 mg/ml for cryo-EM specimen preparation.

For expression and purification of KCTD7, the mouse *KCTD7* gene was amplified from a mouse cDNA library and cloned into pFastBac plasmids with an N-terminal His_6-SUMO-FLAG tag. Sf9 cells were infected with baculovirus at a cell density of 2×10^6 per ml for 2 days. The cells were pelleted, Dounce-homogenized in lysis buffer A, and purified with a Ni-NTA column. The bound fraction was eluted with elution buffer A, incubated overnight with ULP1 on ice, concentrated, and subjected to a Superose 6 increase 10/300 column (Cytiva) equilibrated with equilibration buffer A. The corresponding peak fractions were poured and concentrated for complex assembly. A truncated form of Cul3, Cul3NΔ22 (23-388, I342R, and L346D), was cloned into a pET-Duet plasmid with an N-terminal His_6 tag. The protein was expressed and purified as described above for KCTD5 purification and was further purified with a Superdex 200 increase column equilibrated with equilibration buffer A. To assemble the KCTD7/Cul3 complex, purified KCTD7 and Cul3 were mixed with a molar ratio of 1:1.5 and incubated on ice for 10 min. The complex was subjected to a Superose 6 increase column equilibrated with equilibration buffer A. The peak fractions corresponding to KCTD7/Cul3 complex formation were collected and concentrated to 0.32 mg/ml for cryo-EM sample preparation.

Cryo-EM specimen preparation and data collection

For the KCTD5-$G\gamma_2/G\beta_1$ fusion complex, a glow-charged 300-mesh holey carbon grid (Quantifoil R1.2/1.3 Au) was loaded into a Vitrobot Mark IV chamber (Thermo Fisher Scientific) at 8°C and 100% humidity. A total of 3.0 μl of the concentrated complex

sample was applied onto the grid and blotted for 4.0 s before plunge-freezing in liquid ethane. Cryo-EM images were collected using EPU on a Titan Krios G4 microscope (Thermal Fisher Scientific) equipped with a Falcon 4 direct electron detector and operated at 300 kV at a magnification of ×96,000 with a pixel size of 0.86 Å. Each movie stack was dose-fractionated to 32 frames with a total dose of 49.71 $e^{-}Å^{-2}$ for 5.59 s.

For the KCTD7/Cul3 complex, 3.0 μl of the sample was loaded onto a glow-charged 400-mesh holey grid (Quantifoil R1.2/1.3 Au) coated with graphene oxide and blotted for 2 s with a blot force of 2 followed by plunge-freezing in liquid ethane. The images were collected using EPU on a Titan Krios G3 microscope (Thermal Fisher Scientific) equipped with a BioQuantum GIF/K3 (Gatan) direct electron detector in a super-resolution mode and operated at 300 kV at a magnification of ×64,000 with a pixel size of 1.087 Å. Each movie stack was dose-fractionated to 32 frames with a total dose of 50 $e^{-}Å^{-2}$ for 2.56 s.

Cryo-EM data processing

For the KCTD5-G$\beta_1\gamma_2$ fusion complex, a total of 4354 movie stacks were motion-corrected using MotionCor2 (*56*). Micrographs were imported into CryoSPARC software (*57*) for contrast transfer function (CTF) estimation using patch-based CTF estimation. A total of 3,669,479 particles were picked using Blob Picker, extracted with a 350-pixel box size, and subjected to three rounds of 2D classification. Only 2D classes with typical features of both KCTD5 and Gβγ were selected, resulting in 619,265 particles. These particles were sent to ab initio reconstruction and heterogeneous refinement. One class with five copies of Gβγ was selected for nonuniform (NU) refinement with fivefold (C5) symmetry imposed. The map is not good enough for model building due to the presence of KCTD5 with partially occupied Gβγ and is used as a reference map for the following map calculation. In parallel, particle picking was performed using the Template Picker module in CryoSPARC. After 2D classification, classes with five copies of Gβγ including 413,512 particles were selected and subjected to homogenous refinement. The aligned particles were classified into 10 classes using 3D classification in CryoSPARC with C5 symmetry imposed. One class represents 24% of the total particles exhibiting high-resolution features and was subjected to NU Refinement with C5 symmetry imposed, yielding a final map with a global resolution of 3.3 Å.

For the KCTD7 and Cul3 complex, 358 movie stacks were motion-corrected with MotionCor2 and imported into CryoSPARC software for CTF estimation using the patch CTF estimation module. Using the blob picker module and Topaz particle pick module, a total of 398,489 particles were extracted and sequentially subjected to 2D classification, ab initio reconstruction, NU refinement (C5 symmetry imposed), and local refinement (C5 symmetry imposed), resulting in a map with a global resolution of 2.88 Å.

Model building

Crystal structures of KCTD5 (PDB: 3DRY) and G$\beta_1\gamma_2$ (PDB: 6M8S) were used as templates for the model building of the KCTD5-G$\beta_1\gamma_2$ fusion complex. The CTD of KCTD5 and five copies of Gβγ subunits were fit into the EM map of the KCTD5-Gγ_2/Gβ_1 fusion complex using Chimera (*58*). The model was manually adjusted in COOT 0.9-pre (*59*) before running a real_space_refinement in Phenix (*60*) using secondary structure restraints. For the KCTD7 and Cul3 complex, the crystal structure of Cul3 (6I2M, chain B) was docked into the map using Chimera, and the KCTD7 model was built de novo using COOT 0.9-pre. Side chains with poor EM density maps were chopped. The final model was refined with real_space_refinement in Phenix using the secondary structure restraints. Structure and map figures were prepared using PyMOL, Chimera, and ChimeraX (*61*) software.

FLAG pull-down assays

KCTD2, *KCTD5*, *KCTD17* (isoforms 1 to 4), *Inc*, *KCTD7*, and all mutated and truncated forms were cloned into a pET28a(+) plasmid with N terminal His_6-SUMO and FLAG tags, expressed in *E. coli* BL21 strain (DE3), and purified using the same procedure as described above for KCTD5 purification. After Ni-NTA affinity purification, the eluate was treated with ULP1 to remove the His_6-SUMO tag to expose the FLAG tag before being used for the M1 FLAG pull-down assay.

The Gβ_1 WT and mutants were cloned into pcDNA3.1(+) plasmid with an N-terminal His_6 tag followed by a protein C tag and 3x HA tag. Gγ_2 was cloned into pcDNA3.1(+) plasmid. The plasmids were cotransfected into Expi293F cells at a density of 2 million per milliliter and cultured for 2 days. The cells pelleted were homogenized by a Dounce homogenizer using a Teflon Tissue grinder in hypotonic buffer (20 mM Hepes, pH 7.4) and solubilized in the solubilization buffer [20 mM Hepes (pH 7.4), 150 mM NaCl, 0.5% Lauryl Maltose Neopentyl Glycol (LMNG), and 10 mM imidazole]. Following centrifugation, the clarified lysate was loaded onto a Ni-NTA column pre-equilibrated with a buffer containing 20 mM Hepes (pH 7.4), 150 mM NaCl, and 0.01% LMNG. The bound fraction was washed and eluted with a buffer containing 20 mM Hepes (pH 7.4), 150 mM NaCl, 0.01% LMNG, and 250 mM imidazole. The eluate was supplemented with 2 mM $CaCl_2$, purified again using the protein C antibody affinity resin, and eluted in a buffer containing 20 mM Hepes (pH 7.4), 150 mM NaCl, 0.01% LMNG, 5 mM EDTA, and protein C peptide (0.1 mg/ml).

For KCTDs and Gβγ pull-down assays, 45 μg of KCTDs or mutants and 45 μg of Gβγ or mutants were mixed in wash buffer A [20 mM Hepes (pH 7.4), 120 mM NaCl, 0.01% LMNG, and 2 mM $CaCl_2$] and were incubated on ice for 10 min. The protein mixture was added with 5 μl of M1 FLAG antibody resin and incubated at 4°C for 30 min. The resin was then washed three times with wash buffer A and eluted with a buffer containing 20 mM Hepes (pH 7.4), 120 mM NaCl, 0.01% LMNG, FLAG peptide (0.1 mg/ml), and 1% SDS. Input and eluate samples were separated by SDS-PAGE electrophoresis and stained with Coomassie blue.

For KCTD5 or KCTD7 and Cul3 pull-down assays, 45 μg of KCTD5 or KCTD7 and Cul3 was mixed in wash buffer B [20 mM Hepes (pH 7.4), 250 mM NaCl, and 2 mM $CaCl_2$), and experiments were performed using the same procedure for KCTDs and Gβγ pull-down assay except that the beads were washed with wash buffer B and eluted with a buffer containing 20 mM Hepes (pH 7.4), 250 mM NaCl, FLAG peptide (0.1 mg/ml), and 1% SDS.

Coimmunoprecipitation

For verification of the interaction between KCTD5 and Gβ_1 to Gβ_5 as well as their *D. melanogaster* homologs, human *Gβ1* to *Gβ5* genes were amplified from a cDNA library of a human embryonic kidney (HEK) 293T cell line, while *Gβ13F*, *Gβ76C*, and *Drosophila Gγ* genes

were amplified from a *Drosophila* cDNA library. *KCTD5* and *Gβ* genes were cloned into the pcS2 plasmid with an N-terminal FLAG tag and 3x HA tag, respectively, and *Gγ* genes were cloned into pcS2 plasmids without a tag. HEK293T cells cultured in Dulbecco's modified Eagle's medium supplemented with 10% fetal bovine serum (FBS) under 37°C, 5% CO_2, were seeded into six-well plates and transfected the next day with 0.8 μg of KCTD5, 0.8 μg of Gβ, and 0.8 μg of Gγ plasmids per well using PEI. After 2 days, cells were suspended, washed twice with ice-cold phosphate-buffered saline, and lysed in 300 μl of a buffer containing 20 mM Hepes (pH 7.4), 0.5% LMNG, and Roche protease inhibitor cocktail on ice for 10 min. The lysate was then centrifuged at 20,000*g* for 10 min. The supernatant was mixed with 5 μl of M2 FLAG antibody resin and incubated at 4°C for 1 hour. The resin was then washed five times with wash buffer A and eluted with wash buffer A supplemented with FLAG peptide (0.1 mg/ml) and 1% SDS. The eluate was analyzed by Western blot using anti-FLAG (Sigma-Aldrich) and anti-HA antibodies (Sigma-Aldrich).

In vivo degradation assay

The *KCTD5-KO* cell line was generated using the CRISPR-Cas9 system. The eHAP cells were maintained in RPMI 1640 medium supplemented with 10% FBS. A guide RNA (5′-tcggcttaccttcctccgcg-3′) targeting KCTD5 was annealed into lenti-CRISPR v2 plasmid containing Cas9 expression cassette and puromycin selection marker before lentivirus packing. The eHAP cells were infected and selected with puromycin (2 μg/ml; Invitrogen). Single colonies were picked, and the *KCTD5* gene KO was verified by sequencing. Cells were lysed in 20 mM Hepes (pH 7.4), 150 mM NaCl, and 0.5% LMNG, and the lysate was analyzed by Western blot using anti-KCTD2/5/17 protein antibody (Proteintech). $Gβ_1$ level was probed using an anti-$Gβ_1$ antibody (Abcam). For complementation, the *KCTD5* gene and its mutants, as well as *KCTD2*, *KCTD17*_1 to 4, and *KCTD12* were cloned into pLenti_Blast vector with a FLAG tag and blasticidin selection marker. The eHAP_*KCTD5-KO* cells were infected with lentivirus carrying the complementation constructs and selected with blasticidin (3 μg/ml; Invitrogen). The selected pool was passed for two generations and induced with doxycycline (Dox, 1 μg/ml; Sigma-Aldrich) for 24 hours. The cell lysate was analyzed by Western blot using anti-FLAG and anti-$Gβ_1$ antibodies. Anti–ACTIN-β antibody (Beyotime) was used for a loading control.

Molecular dynamics simulation

MD simulations were performed using GROMACS software (2019.6). The Cul3/Rbx1/KCTD5/Gβγ model was constructed by aligning our KCTD5-Gβγ fusion complex with the crystal structure of KCTD5 (3DRY), the cryo-EM structure of Cul3/KCTD7, the crystal structure of Cul1/Rbx1 (1LDJ), and the structure of Cul3 predicted from AlphaFold (*62*). Missing loops in the KCTD5 CTD region were fixed with ROSETTA suit using the Kinematic Loop Closure (KIC) method (*63*). The model was immersed in a triclinic box of size 28.227 × 34.751 × 25.161 nm^3 with 782,243 water molecules. Forty-five water molecules were replaced with Na^+ to neutralize the system. The system was energy-minimized with 150 mM NaCl and equilibrated at 300 K and 1 atm. The system was then kept at 300 K and run in Amber03 force field for 50 ns. Data were processed using GROMACS, xmgrace, and plotted using GraphPad Prism software. Structures were visualized and plotted using ChimeraX software.

Cyclic adenosine 3′,5′-monophosphate accumulation (cAMP) assay

Two milliliters of *KCTD5*-KO cells was seeded into six-well plates and transfected with KCTDs WT or mutants, D1R, and cAMP Glo-Sensor plasmid by a mass ratio of 1:1:1 to a total amount of 2.5 μg per well using the Lipofectamine 3000 kit. The transfected cells were cultured for 2 days and seeded into white 96-well plates with clear bottom (Corning). After incubation for 12 hours, the culture was refreshed with a CO_2-independent medium supplemented with D-luciferin (0.5 mg/ml; Beyotime). The culture was then equilibrated for 2 hours at room temperature and stimulated with increasing concentrations of dopamine. The bioluminescence signal was constantly monitored for 500 s. For concentration-response curves, the bioluminescence signal at 400 s was plotted as the function of dopamine concentrations and fitted to a three-parameter sigmoidal curve using GraphPad Prism 8 software. All experiments were repeated three independent times, each in triplicate.

Supplementary Materials

This PDF file includes:

Figs. S1 to S7
Table S1
Legend for uncropped SDS-PAGE and western blot gels

Other Supplementary Material for this manuscript includes the following:

Uncropped SDS-PAGE and western blot gels

REFERENCES AND NOTES

1. R. J. Lefkowitz, Seven transmembrane receptors: Something old, something new. *Acta Physiol. (Oxf.)* **190**, 9–19 (2007).
2. A. V. Smrcka, G protein βγ subunits: Central mediators of G protein-coupled receptor signaling. *Cell. Mol. Life Sci.* **65**, 2191–2214 (2008).
3. Y. Lin, A. V. Smrcka, Understanding molecular recognition by G protein βγ subunits on the path to pharmacological targeting. *Mol. Pharmacol.* **80**, 551–557 (2011).
4. D. E. Logothetis, Y. Kurachi, J. Galper, E. J. Neer, D. E. Clapham, The βγ subunits of GTP-binding proteins activate the muscarinic K^+ channel in heart. *Nature* **325**, 321–326 (1987).
5. S. R. Ikeda, Voltage-dependent modulation of N-type calcium channels by G-protein βγ subunits. *Nature* **380**, 255–258 (1996).
6. W. J. Tang, A. G. Gilman, Type-specific regulation of adenylyl cyclase by G protein βγ subunits. *Science* **254**, 1500–1503 (1991).
7. M. Camps, A. Carozzi, P. Schnabel, A. Scheer, P. J. Parker, P. Gierschik, Isozyme-selective stimulation of phospholipase C-beta 2 by G protein βγ subunits. *Nature* **360**, 684–686 (1992).
8. N. J. Freedman, R. J. Lefkowitz, Desensitization of G protein-coupled receptors. *Recent Prog. Horm. Res.* **51**, 319–351 (1996).
9. S. Rajagopal, S. K. Shenoy, GPCR desensitization: Acute and prolonged phases. *Cell. Signal.* **41**, 9–16 (2018).
10. C. A. Moore, S. K. Milano, J. L. Benovic, Regulation of receptor trafficking by GRKs and arrestins. *Annu. Rev. Physiol.* **69**, 451–482 (2007).
11. J. A. Pitcher, J. Inglese, J. B. Higgins, J. L. Arriza, P. J. Casey, C. Kim, J. L. Benovic, M. M. Kwatra, M. G. Caron, R. J. Lefkowitz, Role of βγ subunits of G proteins in targeting the β-adrenergic receptor kinase to membrane-bound receptors. *Science* **257**, 1264–1267 (1992).
12. C. V. Carman, J. L. Parent, P. W. Day, A. N. Pronin, P. M. Sternweis, P. B. Wedegaertner, A. G. Gilman, J. L. Benovic, T. Kozasa, Selective regulation of $Galph_{aq/11}$ by an RGS domain in the G protein-coupled receptor kinase, GRK2. *J. Biol. Chem.* **274**, 34483–34492 (1999).
13. D. T. Lodowski, J. A. Pitcher, W. D. Capel, R. J. Lefkowitz, J. J. G. Tesmer, Keeping G proteins at bay: A complex between G protein-coupled receptor kinase 2 and Gßγ. *Science* **300**, 1256–1262 (2003).

14. A. Raveh, A. Cooper, L. Guy-David, E. Reuveny, Nonenzymatic rapid control of GIRK channel function by a G protein-coupled receptor kinase. *Cell* **143**, 750–760 (2010).
15. H. G. Dohlman, J. Thorner, RGS proteins and signaling by heterotrimeric G proteins. *J. Biol. Chem.* **272**, 3871–3874 (1997).
16. E. M. Ross, T. M. Wilkie, GTPase-activating proteins for heterotrimeric G proteins: Regulators of G protein signaling (RGS) and RGS-like proteins. *Annu. Rev. Biochem.* **69**, 795–827 (2000).
17. X. Teng, A. Aouacheria, L. Lionnard, K. A. Metz, L. Soane, A. Kamiya, J. M. Hardwick, KCTD: A new gene family involved in neurodevelopmental and neuropsychiatric disorders. *CNS Neurosci. Ther.* **25**, 887–902 (2019).
18. Z. Liu, Y. Xiang, G. Sun, The KCTD family of proteins: Structure, function, disease relevance. *Cell Biosci.* **3**, 45 (2013).
19. C. Golzio, J. Willer, M. E. Talkowski, E. C. Oh, Y. Taniguchi, S. Jacquemont, A. Reymond, M. Sun, A. Sawa, J. F. Gusella, A. Kamiya, J. S. Beckmann, N. Katsanis, KCTD13 is a major driver of mirrored neuroanatomical phenotypes of the 16p11.2 copy number variant. *Nature* **485**, 363–367 (2012).
20. G. N. Lin, R. Corominas, I. Lemmens, X. Yang, J. Tavernier, D. E. Hill, M. Vidal, J. Sebat, L. M. Iakoucheva, Spatiotemporal 16p11.2 protein network implicates cortical late mid-fetal brain development and KCTD13-Cul3-RhoA pathway in psychiatric diseases. *Neuron* **85**, 742–754 (2015).
21. C. O. Escamilla, I. Filonova, A. K. Walker, Z. X. Xuan, R. Holehonnur, F. Espinosa, S. Liu, S. B. Thyme, I. A. López-García, D. B. Mendoza, N. Usui, J. Ellegood, A. J. Eisch, G. Konopka, J. P. Lerch, A. F. Schier, H. E. Speed, C. M. Powell, Kctd13 deletion reduces synaptic transmission via increased RhoA. *Nature* **551**, 227–231 (2017).
22. D. M. Pinkas, C. E. Sanvitale, J. C. Bufton, F. J. Sorrell, N. Solcan, R. Chalk, J. Doutch, A. N. Bullock, Structural complexity in the KCTD family of Cullin3-dependent E3 ubiquitin ligases. *Biochem. J.* **474**, 3747–3761 (2017).
23. A. X. Ji, A. Chu, T. K. Nielsen, S. Benlekbir, J. L. Rubinstein, G. G. Privé, Structural insights into KCTD protein assembly and cullin3 recognition. *J. Mol. Biol.* **428**, 92–107 (2016).
24. N. Balasco, L. Pirone, G. Smaldone, S. di Gaetano, L. Esposito, E. M. Pedone, L. Vitagliano, Molecular recognition of Cullin3 by KCTDs: Insights from experimental and computational investigations. *Biochim. Biophys. Acta Proteins Proteom. BBA-Proteins Proteom.* **1844**, 1289–1298 (2014).
25. S. Zheng, N. Abreu, J. Levitz, A. C. Kruse, Structural basis for KCTD-mediated rapid desensitization of $GABA_B$ signalling. *Nature* **567**, 127–131 (2019).
26. H. Zuo, I. Glaaser, Y. Zhao, I. Kurinov, L. Mosyak, H. Wang, J. Liu, J. Park, A. Frangaj, E. Sturchler, M. Zhou, P. McDonald, Y. Geng, P. A. Slesinger, Q. R. Fan, Structural basis for auxiliary subunit KCTD16 regulation of the $GABA_B$ receptor. *Proc. Natl. Acad. Sci. U.S.A.* **116**, 8370–8379 (2019).
27. R. Turecek, J. Schwenk, T. Fritzius, K. Ivankova, G. Zolles, L. Adelfinger, V. Jacquier, V. Besseyrias, M. Gassmann, U. Schulte, B. Fakler, B. Bettler, Auxiliary $GABA_B$ receptor subunits uncouple G protein βγ subunits from effector channels to induce desensitization. *Neuron* **82**, 1032–1044 (2014).
28. J. Schwenk, M. Metz, G. Zolles, R. Turecek, T. Fritzius, W. Bildl, E. Tarusawa, A. Kulik, A. Unger, K. Ivankova, R. Seddik, J. Y. Tiao, M. Rajalu, J. Trojanova, V. Rohde, M. Gassmann, U. Schulte, B. Fakler, B. Bettler, Native $GABA_B$ receptors are heteromultimers with a family of auxiliary subunits. *Nature* **465**, 231–235 (2010).
29. M. Brockmann, V. A. Blomen, J. Nieuwenhuis, E. Stickel, M. Raaben, O. B. Bleijerveld, A. F. M. Altelaar, L. T. Jae, T. R. Brummelkamp, Genetic wiring maps of single-cell protein states reveal an off-switch for GPCR signalling. *Nature* **546**, 307–311 (2017).
30. B. D. Young, J. Sha, A. A. Vashisht, J. A. Wohlschlegel, Human multisubunit E3 ubiquitin ligase required for heterotrimeric G-protein β-subunit ubiquitination and downstream signaling. *J. Proteome Res.* **20**, 4318–4330 (2021).
31. B. S. Muntean, S. Marwari, X. Li, D. C. Sloan, B. D. Young, J. A. Wohlschlegel, K. A. Martemyanov, Members of the KCTD family are major regulators of cAMP signaling. *Proc. Natl. Acad. Sci. U.S.A.* **119**, e2119237119 (2022).
32. Q. Li, D. A. Kellner, H. A. M. Hatch, T. Yumita, S. Sanchez, R. P. Machold, C. A. Frank, N. Stavropoulos, Conserved properties of *Drosophila* Insomniac link sleep regulation and synaptic function. *PLOS Genet.* **13**, e1006815 (2017).
33. K. Kikuma, X. Li, S. Perry, Q. Li, P. Goel, C. Chen, D. Kim, N. Stavropoulos, D. Dickman, *Cul3* and *insomniac* are required for rapid ubiquitination of postsynaptic targets and retrograde homeostatic signaling. *Nat. Commun.* **10**, 2998 (2019).
34. N. Stavropoulos, M. W. Young, *Insomniac* and *Cullin-3* regulate sleep and wakefulness in *Drosophila*. *Neuron* **72**, 964–976 (2011).
35. Q. Li, K. Y. Lim, N. Stavropoulos, Structural and behavioral analysis reveals that Insomniac impacts sleep by functioning as a Cul3 adaptor. *BioRxiv*, (2019).
36. C. Pfeiffenberger, R. Allada, *Cul3* and the BTB adaptor *insomniac* are key regulators of sleep homeostasis and a dopamine arousal pathway in *Drosophila*. *PLOS Genet.* **8**, e1003003 (2012).
37. R. Barfield, H. Wang, Y. Liu, J. A. Brody, B. Swenson, R. Li, T. M. Bartz, N. Sotoodehnia, Y.-D. I. Chen, B. E. Cade, H. Chen, S. R. Patel, X. Zhu, S. A. Gharib, W. C. Johnson, J. I. Rotter, R. Saxena, S. Purcell, X. Lin, S. Redline, T. Sofer, Epigenome-wide association analysis of daytime sleepiness in the Multi-Ethnic Study of Atherosclerosis reveals African-American-specific associations. *Sleep* **42**, zsz101 (2019).
38. N. E. Mencacci, I. Rubio-Agusti, A. Zdebik, F. Asmus, M. H. R. Ludtmann, M. Ryten, V. Plagnol, A. K. Hauser, S. Bandres-Ciga, C. Bettencourt, P. Forabosco, D. Hughes, M. M. P. Soutar, K. Peall, H. R. Morris, D. Trabzuni, M. Tekman, H. C. Stanescu, R. Kleta, M. Carecchio, G. Zorzi, N. Nardocci, B. Garavaglia, E. Lohmann, A. Weissbach, C. Klein, J. Hardy, A. M. Pittman, T. Foltynie, A. Y. Abramov, T. Gasser, K. P. Bhatia, N. W. Wood, A missense mutation *in KCTD17* causes autosomal dominant myoclonus-dystonia. *Am. J. Hum. Genet.* **96**, 938–947 (2015).
39. M. Boada, C. Antúnez, R. Ramírez-Lorca, A. L. De Stefano, A. González-Pérez, J. Gayán, J. López-Arrieta, M. A. Ikram, I. Hernández, J. Marín, J. J. Galán, J. C. Bis, A. Mauleón, M. Rosende-Roca, C. Moreno-Rey, V. Gudnasson, F. J. Morón, J. Velasco, J. M. Carrasco, M. Alegret, A. Espinosa, G. Vinyes, A. Lafuente, L. Vargas, A. L. Fitzpatrick; Alzheimer's Disease Neuroimaging Initiative, L. J. Launer, M. E. Sáez, E. Vázquez, J. T. Becker, O. L. López, M. Serrano-Ríos, L. Tárraga, C. M. van Duijn, L. M. Real, S. Seshadri, A. Ruiz, ATP5H/KCTD2 locus is associated with Alzheimer's disease risk. *Mol. Psychiatry* **19**, 682–687 (2014).
40. T. Fritzius, R. Turecek, R. Seddik, H. Kobayashi, J. Tiao, P. D. Rem, M. Metz, M. Kralikova, M. Bouvier, M. Gassmann, B. Bettler, KCTD Hetero-oligomers confer unique kinetic properties on Hippocampal $GABA_B$ receptor-induced K^+ currents. *J. Neurosci.* **37**, 1162–1175 (2017).
41. R. Seddik, S. P. Jungblut, O. K. Silander, M. Rajalu, T. Fritzius, V. Besseyrias, V. Jacquier, B. Fakler, M. Gassmann, B. Bettler, Opposite effects of KCTD subunit domains on $GABA_B$ receptor-mediated desensitization. *J. Biol. Chem.* **287**, 39869–39877 (2012).
42. X. Teng, S. Chen, Q. Wang, Z. Chen, X. Wang, N. Huang, S. Zheng, Structural insights into G protein activation by D1 dopamine receptor. *Sci. Adv.* **8**, eabo4158 (2022).
43. I. S. Dementieva, V. Tereshko, Z. A. McCrossan, E. Solomaha, D. Araki, C. Xu, N. Grigorieff, S. A. N. Goldstein, Pentameric assembly of potassium channel tetramerization domain-containing protein 5. *J. Mol. Biol.* **387**, 175–191 (2009).
44. D. Barone, N. Balasco, L. Vitagliano, KCTD5 is endowed with large, functionally relevant, interdomain motions. *J. Biomol. Struct. Dyn.* **34**, 1725–1735 (2016).
45. M. R. Whorton, R. MacKinnon, X-ray structure of the mammalian GIRK2 – βγ G-protein complex. *Nature* **498**, 190–197 (2013).
46. E. S. Zimmerman, B. A. Schulman, N. Zheng, Structural assembly of cullin-RING ubiquitin ligase complexes. *Curr. Opin. Struct. Biol.* **20**, 714–721 (2010).
47. M. Zhuang, M. F. Calabrese, J. Liu, M. B. Waddell, A. Nourse, M. Hammel, D. J. Miller, H. Walden, D. M. Duda, S. N. Seyedin, T. Hoggard, J. W. Harper, K. P. White, B. A. Schulman, Structures of SPOP-substrate complexes: Insights into molecular architectures of BTB-Cul3 ubiquitin ligases. *Mol. Cell* **36**, 39–50 (2009).
48. P. Canning, C. D. O. Cooper, T. Krojer, J. W. Murray, A. C. W. Pike, A. Chaikuad, T. Keates, C. Thangaratnarajah, V. Hojzan, B. D. Marsden, O. Gileadi, S. Knapp, F. von Delft, A. N. Bullock, Structural basis for Cul3 protein assembly with the BTB-Kelch family of E3 ubiquitin ligases. *J. Biol. Chem.* **288**, 7803–7814 (2013).
49. K. Baek, D. T. Krist, J. R. Prabu, S. Hill, M. Klügel, L.-M. Neumaier, S. von Gronau, G. Kleiger, B. A. Schulman, NEDD8 nucleates a multivalent cullin-RING-UBE2D ubiquitin ligation assembly. *Nature* **578**, 461–466 (2020).
50. D. M. Duda, D. C. Scott, M. F. Calabrese, E. S. Zimmerman, N. Zheng, B. A. Schulman, Structural regulation of cullin-RING ubiquitin ligase complexes. *Curr. Opin. Struct. Biol.* **21**, 257–264 (2011).
51. Y. Chen, Z. Yang, M. Meng, Y. Zhao, N. Dong, H. Yan, L. Liu, M. Ding, H. B. Peng, F. Shao, Cullin mediates degradation of RhoA through evolutionarily conserved BTB adaptors to control actin cytoskeleton structure and cell movement. *Mol. Cell* **35**, 841–855 (2009).
52. K. Singh, J. Y. Ju, M. B. Walsh, M. A. Dilorio, A. C. Hart, Deep conservation of genes required for both *Drosphila melanogaster* and *Caenorhabditis elegans* sleep includes a role for dopaminergic signaling. *Sleep* **37**, 1439–1451 (2014).
53. R. M. Chemelli, J. T. Willie, C. M. Sinton, J. K. Elmquist, T. Scammell, C. Lee, J. A. Richardson, S. C. Williams, Y. Xiong, Y. Kisanuki, T. E. Fitch, M. Nakazato, R. E. Hammer, C. B. Saper, M. Yanagisawa, Narcolepsy in orexin knockout mice: Molecular genetics of sleep regulation. *Cell* **98**, 437–451 (1999).
54. L. Lin, J. Faraco, R. Li, H. Kadotani, W. Rogers, X. Lin, X. Qiu, P. J. de Jong, S. Nishino, E. Mignot, The sleep disorder canine narcolepsy is caused by a mutation in the *Hypocretin (Orexin) Receptor 2* gene. *Cell* **98**, 365–376 (1999).
55. C. G. Vecsey, G. S. Baillie, D. Jaganath, R. Havekes, A. Daniels, M. Wimmer, T. Huang, K. M. Brown, X.-Y. Li, G. Descalzi, S. S. Kim, T. Chen, Y.-Z. Shang, M. Zhuo, M. D. Houslay, T. Abel, Sleep deprivation impairs cAMP signalling in the hippocampus. *Nature* **461**, 1122–1125 (2009).
56. S. Q. Zheng, E. Palovcak, J.-P. Armache, K. A. Verba, Y. Cheng, D. A. Agard, MotionCor2: Anisotropic correction of beam-induced motion for improved cryo-electron microscopy. *Nat. Methods* **14**, 331–332 (2017).

57. A. Punjani, J. L. Rubinstein, D. J. Fleet, M. A. Brubaker, CryoSPARC: Algorithms for rapid unsupervised cryo-EM structure determination. *Nat. Methods* **14**, 290–296 (2017).
58. E. F. Pettersen, T. D. Goddard, C. C. Huang, G. S. Couch, D. M. Greenblatt, E. C. Meng, T. E. Ferrin, UCSF Chimera—A visualization system for exploratory research and analysis. *J. Comput. Chem.* **25**, 1605–1612 (2004).
59. P. Emsley, K. Cowtan, Coot: Model-building tools for molecular graphics. *Acta Crystallogr. D Biol. Crystallogr.* **60**, 2126–2132 (2004).
60. P. D. Adams, P. V. Afonine, G. Bunkóczi, V. B. Chen, I. W. Davis, N. Echols, J. J. Headd, L.-W. Hung, G. J. Kapral, R. W. Grosse-Kunstleve, A. J. McCoy, N. W. Moriarty, R. Oeffner, R. J. Read, D. C. Richardson, J. S. Richardson, T. C. Terwilliger, P. H. Zwart, *PHENIX*: A comprehensive Python-based system for macromolecular structure solution. *Acta Crystallogr. D Biol. Crystallogr.* **66**, 213–221 (2010).
61. E. F. Pettersen, T. D. Goddard, C. C. Huang, E. C. Meng, G. S. Couch, T. I. Croll, J. H. Morris, T. E. Ferrin, UCSF ChimeraX: Structure visualization for researchers, educators, and developers. *Protein Sci.* **30**, 70–82 (2021).
62. J. Jumper, R. Evans, A. Pritzel, T. Green, M. Figurnov, O. Ronneberger, K. Tunyasuvunakool, R. Bates, A. Žídek, A. Potapenko, A. Bridgland, C. Meyer, S. A. A. Kohl, A. J. Ballard, A. Cowie, B. Romera-Paredes, S. Nikolov, R. Jain, J. Adler, T. Back, S. Petersen, D. Reiman, E. Clancy, M. Zielinski, M. Steinegger, M. Pacholska, T. Berghammer, S. Bodenstein, D. Silver, O. Vinyals, A. W. Senior, K. Kavukcuoglu, P. Kohli, D. Hassabis, Highly accurate protein structure prediction with AlphaFold. *Nature* **596**, 583–589 (2021).
63. R. Das, D. Baker, Macromolecular modeling with rosetta. *Annu. Rev. Biochem.* **77**, 363–382 (2008).

Acknowledgments: We thank F. Shao at NIBS for critical reading of the manuscript. We thank T. Han at NIBS for providing eHAP cell line, lenticrisprV2 plasmids, plenti-blasticidin-Tet-on system, and the lentivirus packing system. We thank T. Wang at NIBS for providing the cDNA library of flies. We thank the staff at Shuimu BioSciences for helping with cryo-EM data collection. **Funding:** This work was funded by Chinese Ministry of Science and Technology, Beijing Municipal Science & Technology Commission and Tsinghua University. **Author contributions:** W.J. and W.W. purified the protein complex, collected cryo-EM data, and performed cryo-EM data processing. W.J. performed model building and all functional assays. The study was supervised by S.Z. The manuscript was written by S.Z. and W.J. with important inputs from Y.K. **Competing interests:** The authors declare that they have no competing interests. **Data and materials availability:** The atomic structures have been deposited at the Protein Data Bank (PDB) under the accession codes 8JKB and 8I79. The EM maps have been deposited at the Electron Microscopy Data Bank (EMDB) under the accession numbers EMD-36367 and EMD-35212. All data needed to evaluate the conclusions in the paper are present in the paper and/or the Supplementary Materials.

Submitted 24 January 2023
Accepted 14 June 2023
Published 14 July 2023
10.1126/sciadv.adg8369